Work Package 5: How are air masses transported through the tropopause?

The main objective is the investigation of the complex interaction between troposphere and stratosphere. A key point to the understanding of this important aspect of the dynamics and the chemistry of the atmosphere is the exchange of air masses across the tropopause (e.g. transport of water vapour into the tropical stratosphere from below or of stratospheric air masses into the mid latitudinal troposphere).

Contribution of DLR

Quantifying the large-scale transport of ozone and water vapour through the thermal tropopause

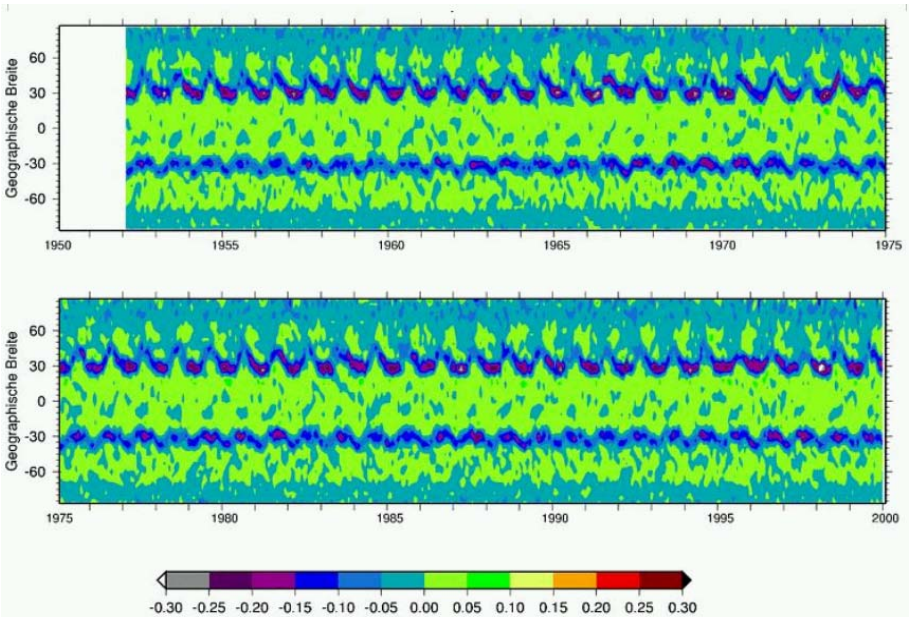

Figure WP5-1: Zonal mean mass flux of ozone through the thermal tropopause as simulated with E39/C (transient simulaton). Negative values denote a mass flux from the stratosphere into the troposphere. Units are 10^{-9} kg m^{-2} s^{-1}.

Data of the transient simulation carried out with the CCM E39/C (see also WPs 1, 3, 4, and 6) have been used to calculate and analyse the mass flux of chemical constituents through the tropopause. The results for the large-scale mass fluxes of water vapour and ozone are displayed in figures WP5-1 and WP5-2. The mass fluxes are estimated employing the formulation firstly described by Wei (1987); here the thermal definition of the tropopause has been used and the model data have been provided in a z-coordinate system. For details see Grewe and Dameris (1996). The mass fluxes in the sub-tropical regions show a pronounced annual cycle, in particular in the latitudinal region between 20° and 70° of both hemispheres, which reflects the movement of the Hadley cells. Ozone is mainly transported from the stratosphere into the troposphere at lower latitudes (approx. 20° to 35°) during spring months, and at middle latitudes (approx. 35° to 50°) during fall months. In other geographical regions and seasons ozone is mostly transported from the troposphere into the stratosphere. The largest transport of water vapour (in winter around 35° latitude; in summer/fall around 50°) is directed from the troposphere into the stratosphere. At first sight, the results presented in figures WP5-1 and -2 seems to be in contradiction, but this is not the case. The transition zone of upward and downward transport of air masses is very sharp (Grewe and Dameris, 1996) and the reverse vertical gradients of ozone and water vapour are causing this overall consistent result.

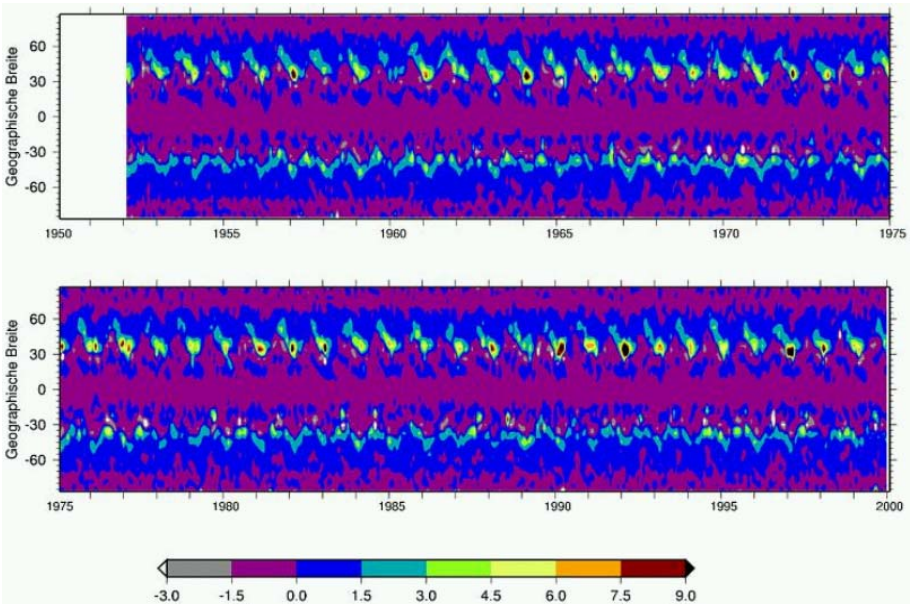

Figure WP5-2: Zonal mean mass flux of water vapour through the thermal tropopause as calculated with E39/C (transient simulation). Negative values denote a mass flux from the stratosphere into the troposphere. Units are 10^{-8} kg m^{-2} s^{-1}.

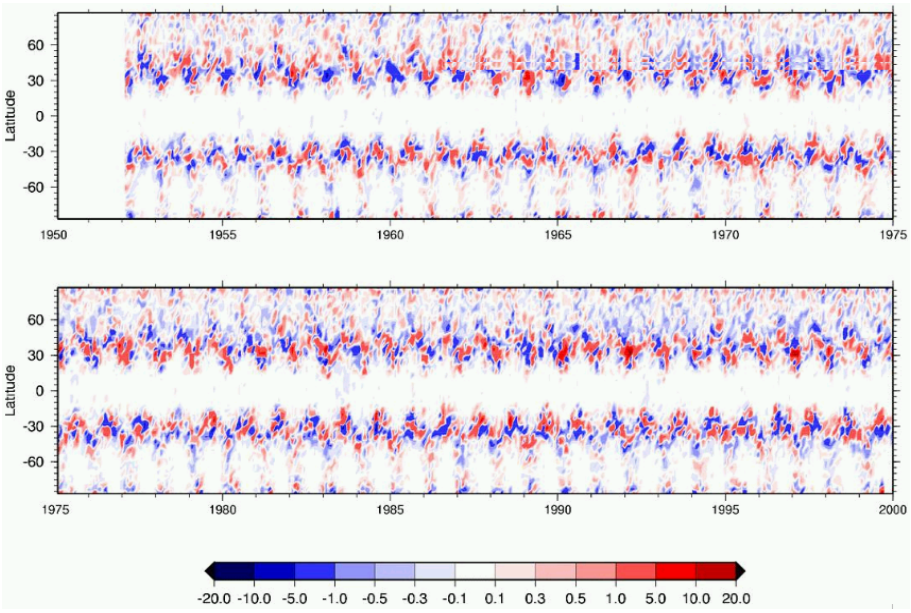

Figure WP 5-3: Anomalies of zonal mean mass flux of water vapour through the thermal tropopause as calculated with E39/C (transient simulation), relativ to the means of the year 1960 to 1980. Units are 10^{-8} kg m^{-2} s^{-1}.

The calculated mass fluxes are generally larger in the Northern Hemisphere than in the Southern Hemisphere. Looking at respective anomalies of the large-scale mass fluxes (related to the means of the years 1960 to 1980), long-term changes and variability can be estimated. Figure WP5-3 illustrates the anomalies of the water vapour mass flux. Largest variability is found around 30° to 40° in both hemispheres, a trend in large-scale mass fluxes cannot be identified.

Contribution of FZJ

Lagrangian modelling of vertical transport and chemical ozone destruction (LAVERO)

Dynamical processes in the tropopause region substantially modify the distribution of chemically and radiatively active atmospheric constituents, thus having a strong impact on the chemistry of the upper troposphere and lower stratosphere and on the climate. The main objective within work package 5 was the investigation of the complex interaction between troposphere and stratosphere. A key point to the understanding of this important aspect of the dynamics and the chemistry of the atmosphere is the exchange of air masses across the tropopause (e. g. transport of water vapor into the tropical stratosphere from below or of stratospheric air masses into the mid latitudinal troposphere).

The vertical transport resulting from both, vertical advection and the effects of diffusivity induced by mixing processes, was investigated with the Chemical Lagrangian Model of the Stratosphere CLaMS (see McKenna et al (2001a) and McKenna et al. (2001b)). At the beginning of KODYACS (and LAVERO) the novel mixing concept of CLaMS was confined to two dimensions thus prohibiting long term calculations with significant vertical displacement of the air masses considered. The mixing concept was extended to three dimensions. This was done by applying the triangulation algorithm to air masses within a layer of a certain vertical extension, thus introducing a vertical grid. The vertical gridding is changed at every mixing time step to avoid the results being biased.

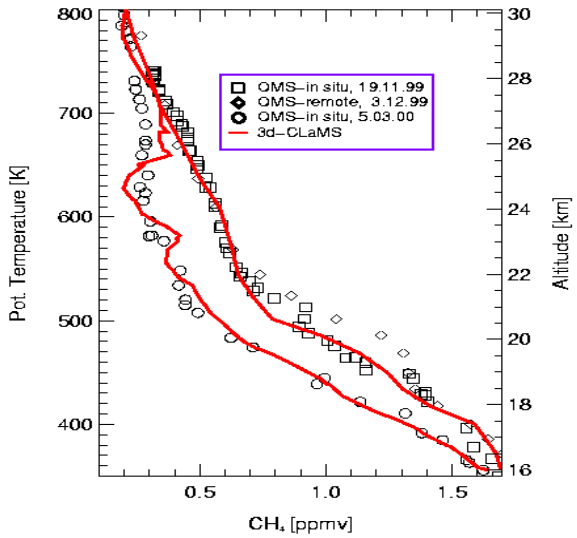

Figure WP 5-4: Results from a CLaMS-3d simulation for the arctic winter 1999/2000 in comparison with ballone bourne methane observations (Konopka et al., 2004).

First results of CLaMS utilizing this new mixing algorithm are presented in Figure WP 5-4. A simulation was started at December 1st, 1999, and carried out until March 5th, 2000, covering the time range of the SOLVE campaign. Vertical profiles of methane derived from measurements made onboard the OMS balloon payload flown on the November 19th, December 3rd and March 5th (see Ray et al, 2002) is shown together with profiles resulting from the model simulation (red lines). Given the uncertainties in model initialization and the length of the simulation period, which is quite long for a trajectory calculation, there was in general a remarkable good agreement between measurement and model results. Although this simulation was carried out mainly for the lower stratosphere, it is shown here to demonstrate the capabilities of CLaMS to model vertical transport. For more details about this simulation and more results about mixing and ozone loss during this episode refer to Konopka et al. (2004).

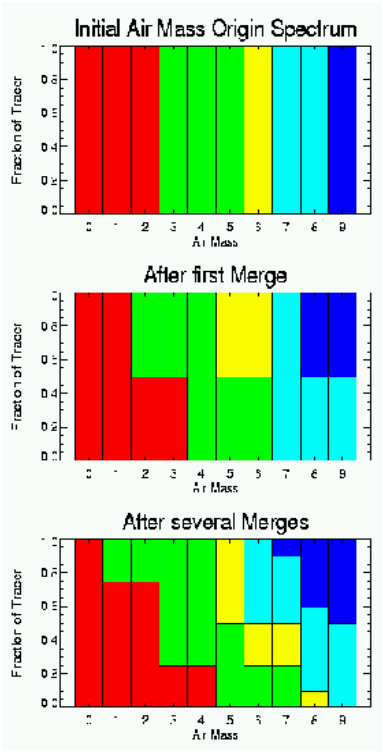

Figure WP 5-5: Air masses are initialized with inert tracers depending on the values of e. g. (m)PV or latitude at their positions at the beginning of the simulation, shown as different colours in the diagram to the left. During the course of the simulation mixing leads to merging and creation of air parcels, thus interchanging information of original properties. At the end of the simulation every air mass has its own spectrum of tracers, indicating the origin of all ancestral air masses that contributed to its composition.

The effects of cross-tropopause transport by advection and mixing processes were then studied with the improved CLaMS using ECMWF analysis data. The results discussed hereafter are inferred from high resolution hemispherical simulations based on trajectory calculations with mixing between the considered air parcels. Mixing processes are simulated by merging already existing air parcels or creating new air parcels when the distances between air parcels are below a minimum radius or above a certain maximum radius, respectively. The change in composition of air masses due to mixing is analysed by utilization of inert artificial tracers marking the different air mass origins (e. g. tropospheric vs. stratospheric). Due to mixing the contents of merged or newly created air parcels is changed, thus reflecting the origins of the contributing air masses. Thereby a spectrum of air mass origin for every single air parcel is created, that is determined by its mixing history during the course of the simulation (see Fig. WP 5-5). Analyses of these spectra help to investigate stratospheric and tropospheric influences on observed air masses or to quantify stratospheric-tropospheric-exchange. Additionally the distribution of water vapour is simulated. For this purpose a simple model parameterizing the formation, sedimentation and evaporation of cirrus clouds particles was introduced into CLaMS. The initialization of water vapour is taken from ECMWF data.

The hemispheric simulations between 300 K and 450 K were driven by ECMWF data, started three month before the first SPURT campaign in August 2001, and ended in April 2003. The vertical velocity was computed from ECMWF data using temperature and pressure tendencies of subsequent time levels instead of using the values provided in the data sets. Tracers being initialized by the initial PV value (P0,..,P4) and the latitudinal position (L0,..,L5) of the air masses were used. Ice particles were formed at 110 % oversaturation. Sensitivity runs with different oversaturation conditions and a temperature offset of +2K were carried out additionally. Results from these runs are not shown explicitly.

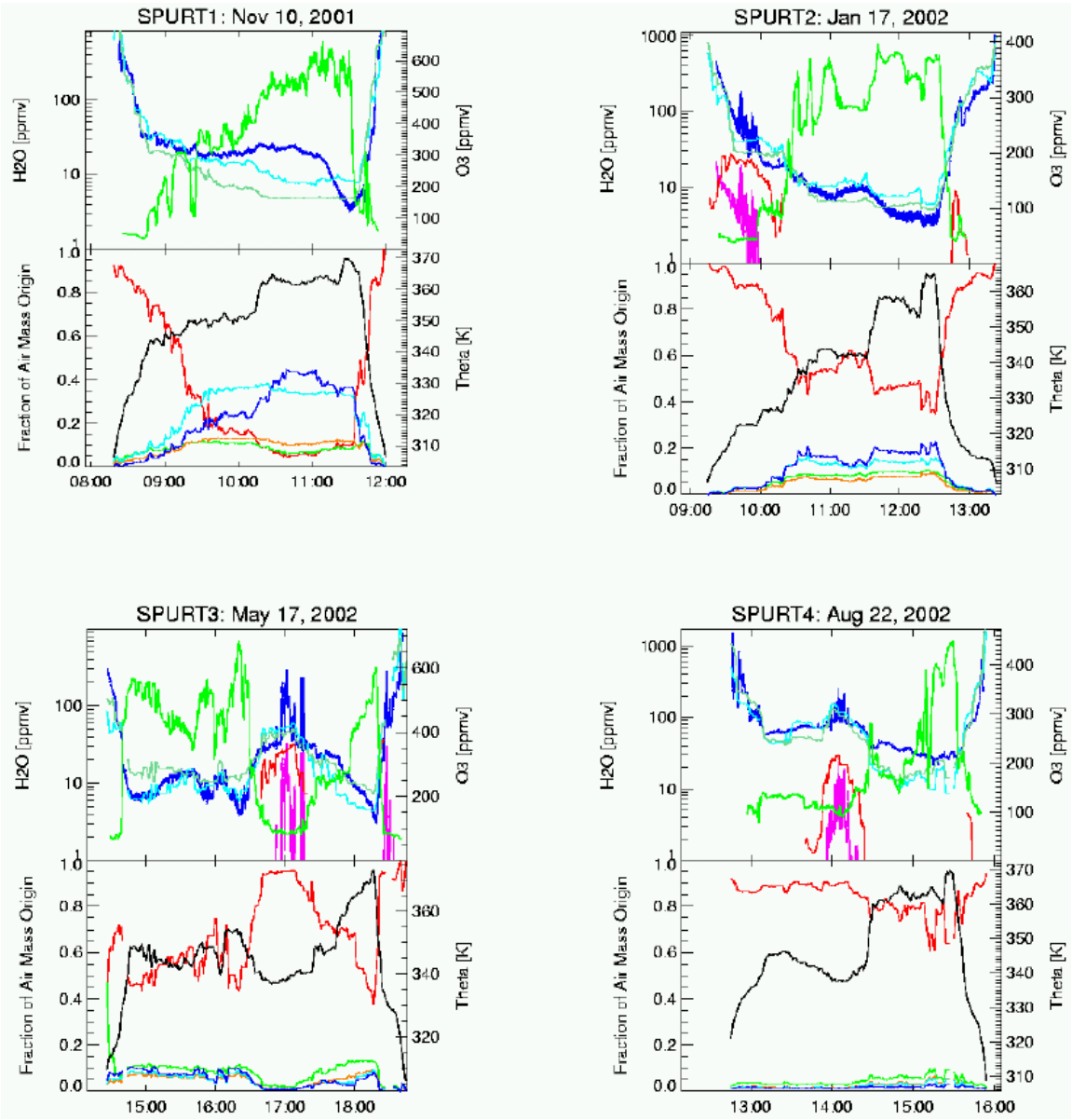

Figure WP 5-6: A comparison between observed water vapour and ozone with CLaMS results and ECMWF data for some flights of the SPURT campaigns 1-4. The upper panel of every plot shows observed water vapour (gas and condensed phase) and ozone measured by the FISH and JOE instruments, respectively, together with water vapour and ice water content as simulated by CLaMS and water vapour taken from ECMWF data along the flight path (see upper legend for colour colour coding). The lower panel displays the potential temperature in K together with the distribution of CLaMS' PV initialized tracers along the flight path, indicating tropospheric and stratospheric influences on the air masses observed during the flight (see legend in Fig. WP 5-7 for colour coding).

The results of the CLaMS simulation regarding the inert tracers and water in both condensed and gas phase are in good agreement with ozone and water vapour observations made during SPURT (see Figs. WP 5-6 and 7). Stratospheric air masses in the model are often moister than observed, indicating a perhaps too strong mixing. The most prominent exceptions are the observations made during SPURT 6 and 7, where unusual high water was observed in the stratosphere. The results of sensitivity runs carried out with different oversaturation conditions and a temperature offset of +2K could not reproduce these high water values.

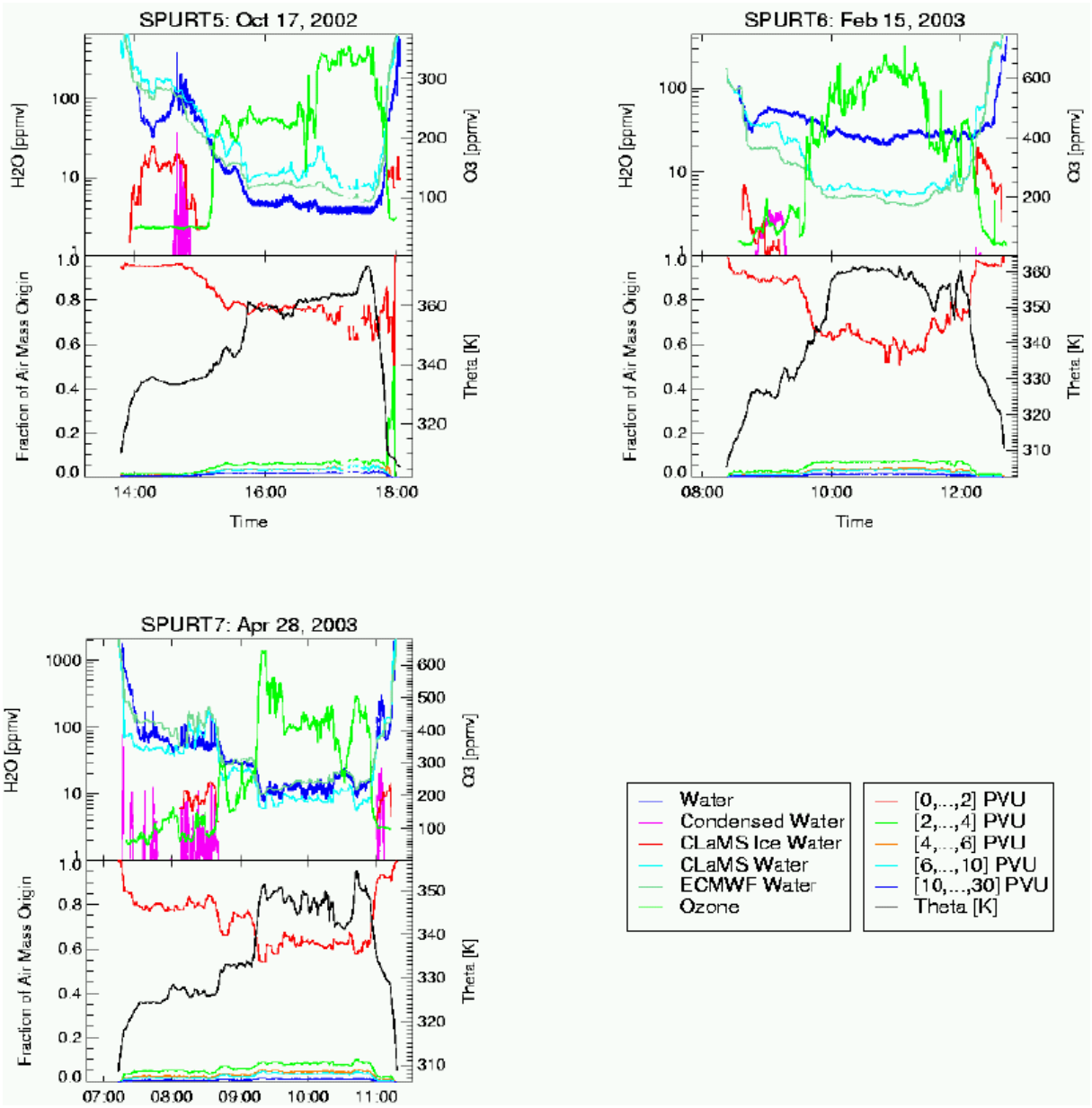

Figure WP 5-7: as figure WP 5-6, but for SPURT campaigns 5-7.

The distribution of water vapour and the tropospheric tracer P0 in a certain along the flight path (Fig. WP 5-8) shows air masses dryer than observed, but with a tropospheric influence of 50 to 60 % suggesting a potential of higher water vapor.

An analysis of the complete air mass origin spectra of simulated air masses for this flight (Fig. WP 5-9) indicates that the air observed was not only under considerable tropospheric influence but was originally located mainly in the tropics. After having been moved into the mid latitudes these air masses were mixed with air from higher up in the stratosphere.

The UTLS region over the North Atlantic and Europe was heavily disturbed by a series of consecutive upper tropospheric lows forming troughs and ridges in the lower stratosphere during February 2002, thus leading to enhanced meridional transport moving moist air from the subtropics into the lowermost stratosphere, followed by rapid mixing with dry stratospheric air (Fig. WP 5-10). A possible explanation for the fact, that the model atmosphere is less moist over Europe than observed may be too strong mixing and/or a too dry model stratosphere.

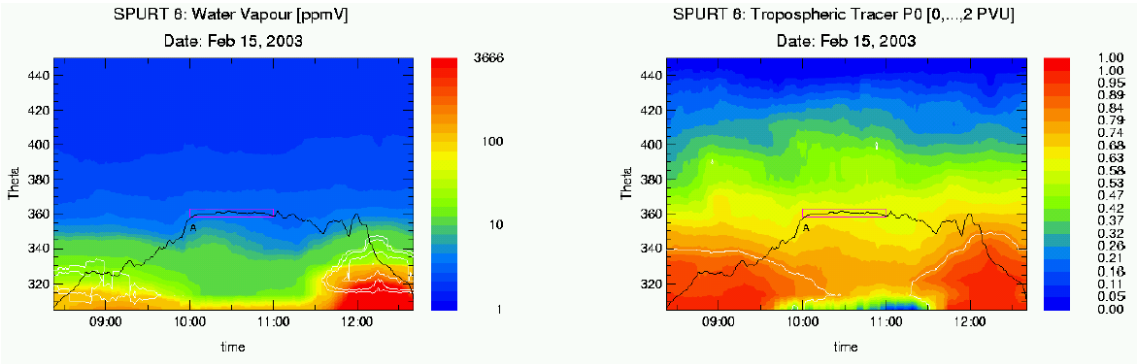

Figure WP 5-8: The distribution of water vapour and ice water content (left) and the tracer P0, indicating tropospheric influence (right), in a curtain along the flight path on the 15th of February, 2003, as simulated by CLaMS. The white lines correspond to contours (1.,2.,5.,10.,20. ppmv) of ice water content (left) and the 2 PVU contour line (right) indicating the position of the tropopause.

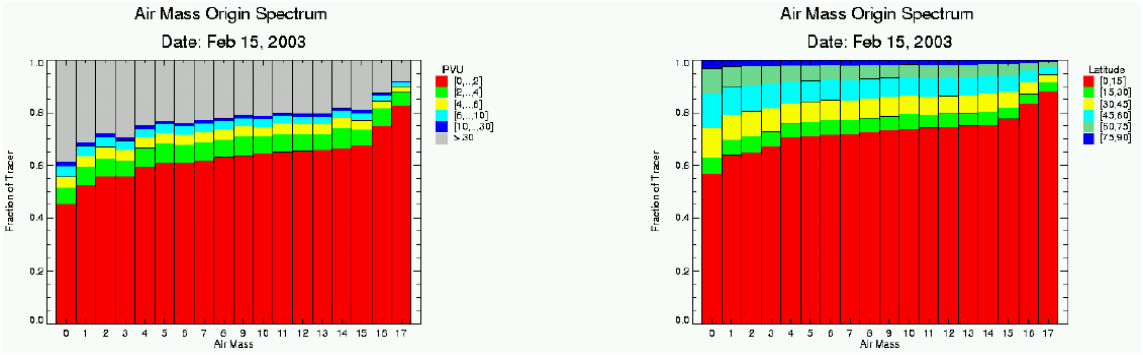

Figure WP 5-9: The air mass origin spectra for PV-initialized (left) and latitude-initialized (right) tracers of air masses along the flight path in the area indicated by the pink box in Fig. WP 5-8.

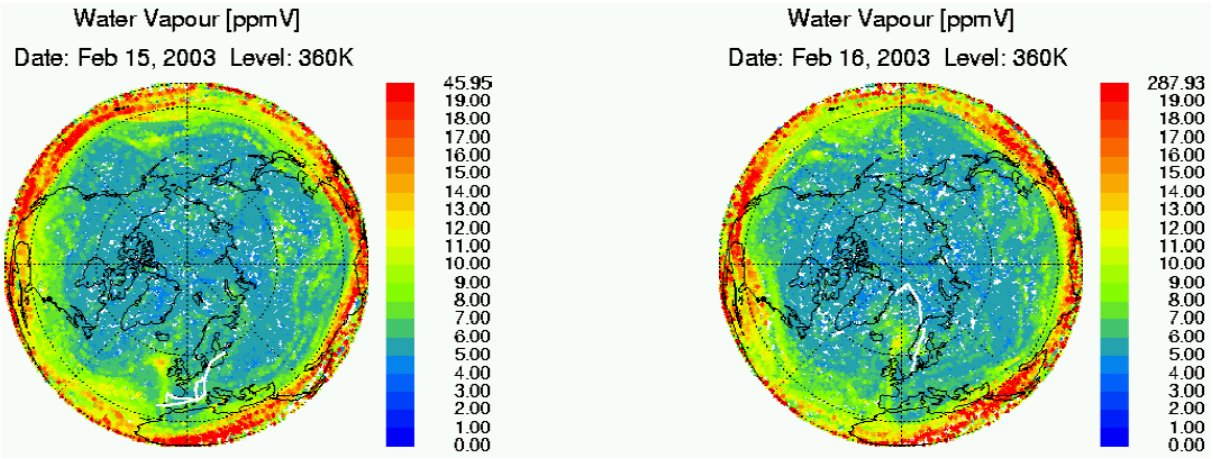

Figure WP 5-10: Horizontal distribution of simulated water vapour for February 15th and 16th on the 360 K level. The white lines correspond to the flight paths of the four flights carried out on these two days.

The evolution of the tropospheric tracer P0 during the simulation (Fig. WP 5-11, left column) shows the different ways air enters the stratosphere: While a mixing layer with an average height of about 20 K in the vicinity of the tropopause is formed within a few weeks, the slower transport across the tropical tropopause needs on the order of month to establish. During winter the UTLS is characterized by the Brewer-Dobson circulation with strong upward transport in the tropics, poleward motion in the lower stratosphere and downward transport of stratospheric air over the polar regions. Below the core of the subtropic jet stratospheric air is mixed into the troposphere. These transport processes lead to a steepening of the meridional gradient of P0. The simulated water vapour (Fig. WP 5-11, right column) shows low values in the lowermost stratosphere and an extremely dry tropical tropopause.

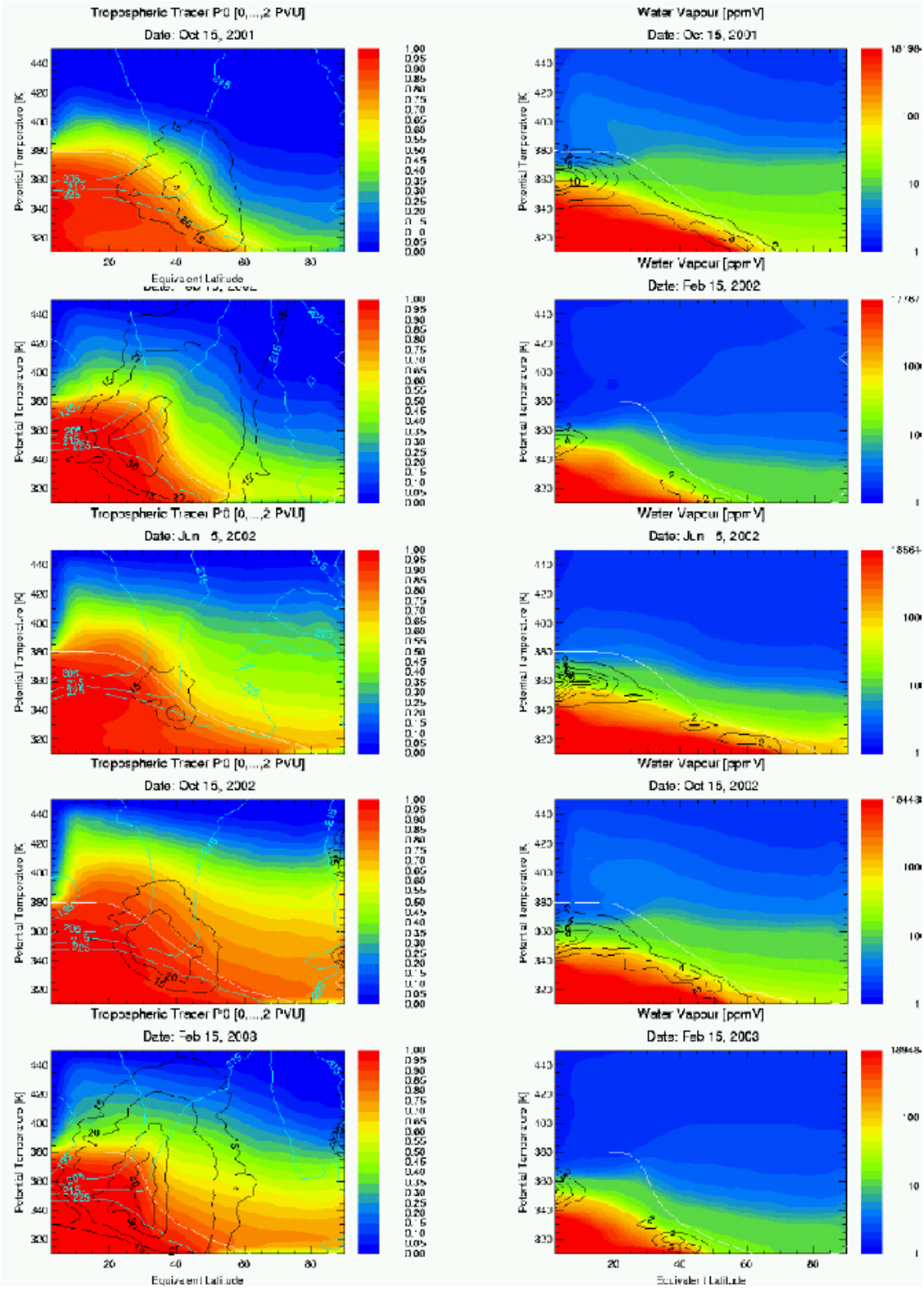

Figure WP 5-11: Equivalent zonal mean of tropospheric tracer P0 together with temperature in K (cyan) and zonal wind in m/s (black)(left column), and water vapour together with ice water content (black) (right column). The white line corresponds to the tropopause defined by 4 PVU.

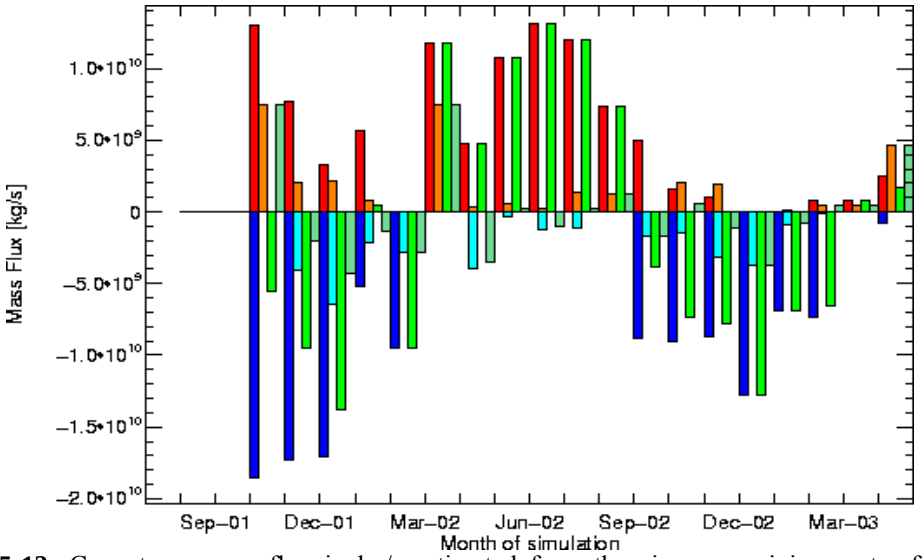

Figure WP 5-12: Cross-tropopause flux in kg/s estimated from the air mass origin spectra for the whole simulation. Upward fluxes (TST) for the Northern Hemisphere (NH) and the tropics south of 30°N (TR) are shown in red and orange,respectively. Downward fluxes (STT) are in blue (NH) and cyan (TR), net fluxes are in green (NH) and aquamarine (TR). The tropopause was computed from ECMWF data using a value of 2 PVU.

During summer when the subtropical barrier is weakened, isentropic transport and mixing lead to an enhancement of tropospheric influence in the lowermost stratosphere, thus increasing water vapour in the extratropical lowermost stratosphere. Significant tropospheric influence can be seen up to 400 K. Due to strong convection the tropical tropopause region shows a maximum in the occurence of cirrus clouds. In the vicinity of the extratropical tropopause cirrus clouds can contain about 40% of the total water content, thus contributing significantly to the transport of water vapour into the stratosphere.

During late winter and early spring 2003 strong perturbations of the UTLS lead to an enhanced transport of troposheric air into the lowermost stratosphere, creating small scale structures and filaments of moist air, thus increasing the water vapour locally to values around 20 to 30 ppmv (see Figs. WP 5-6, 7 and 11). It seems that the mixing in CLaMS works too efficiently in reducing these small scale structures by eroding them and creating an elevated background of water vapour.
With the help of the spectra of air mass origins it is possible to give an estimate of the cross-tropopause flux in the model atmosphere (Fig. WP 5-12). This was carried out by integrating over the tropospheric (stratospheric) parts of air masses in the stratosphere (troposphere). Since the spectra loose their significance concerning direct transport across the tropopause the longer the simulation carries on, the fluxes were deduced from month-to-month changes of the tracer budgets. The first months were ommitted due to the unrealistic fluxes occuring during the establishing of the mixing layer in the spin-up phase of the model.

The results of the contributions of FZ Jülich to work package 5 can be summarized as follows:

- In the beginning of the project a 3-dimensional version of the Chemical Lagrangian Model of the Stratosphere CLaMS was completed and utilized in various model simulations.
- The first 21-month-simulation with CLaMS was carried out for almost the whole SPURT episode from August 2001 until April 2003. The results concerning water vapour and ice water content are in good agreement with observations obtained during SPURT.
- The simple model implemented to parameterize the formation, evaporation and sedimentation of cirrus particles worked successfully.
- Model results and observations suggest that the lowermost stratosphere can be moister than expected during episodes with enhanced meridional transport.
- Transport and evaporation of cirrus particles can contribute up to 50% to the stratospheric water vapour values locally.

- The utilization of inert tracers allows the quantification of
    - Mixing on short time scales
    - Flux of air masses across the tropopause

Future works will include the further development of the cirrus and cloud model, to investigate the influence of cloud water and particles on the water budget of the UTLS region. More long term simulations will be carried out to build a climatology of CLaMS. This has to be compared to observations, both in situ and remote sensing, to validate and calibrate the model and its parameters.

Contribution of IMK-KASIMA

KASIMA model description

The Karlsruhe Simulation Model of the Middle Atmosphere (KASIMA) model is a global circulation model including stratospheric chemistry for the simulation of the behaviour of physical and chemical processes in the middle atmosphere. The meteorological component is based on a spectral architecture with the pressure altitude $z = H \ln(p/p_0)$ as vertical coordinate, where $H = 7$ km is a constant scale height and p and $p_0 = 1013{,}25$ hPa are pressure and a constant reference pressure, respectively. The meteorology module of the KASIMA model consists of three versions: the diagnostic model, the prognostic model and the nudged model which combines the prognostic and diagnostic model (Kouker et al., 1999).

For these experiments, the nudged model is used only, and a spatial resolution is mostly set to T106 in the horizontal and 25 layers between 3 and 25 km altitude. This model version treats KASIMA as an adiabatic primitive equation model which has as non-conservative term a Netownian cooling term which nudges the temperature by a net heating rate towards the analysed temperature. The term can then beregarded as a crude parameterization of processes like latent heat releases, which have their impact at first in the thermodynamic equation.

Deveopment of an analyses scheme for complex structured surfaces

The quantitative analyses of isosurfaces rely on conventions founded in various disciplines of computational geometry (e.g. O'Rourke, 1994). Geometric structures are described by a set of vertices and polyhedra obtained by triangulation (tetrahedrals or triangles for 3D or 2D structures, respectively).The following steps are undertaken for the analyses:

- The 3D model domain spanned as a regular grid in KASIMA is triangulated. The space between neighbored gridpoints in each direction is seen as an idealize cubbe, which itself is triangulated in a set of 6 tetrahedrals as visualized in figure 5-13. Thus, the vertices of all tetrahedrals are the model gridpoints.
- Each tetrahedral can be truncated by an isosurface only once. The isosurface element is obtained from linear interpolation along the edges of each tetrahedral.
- Gradients within the tetrahedrals are computed from linear differencing along the edges of each tetrahedral. Thus, the gradient of the 3-d field the isosurface is analysed of is allways perpendicular to the isosurface, which is not generally achieved when gradients are obtain e.g. from differences along the edges of the cube.

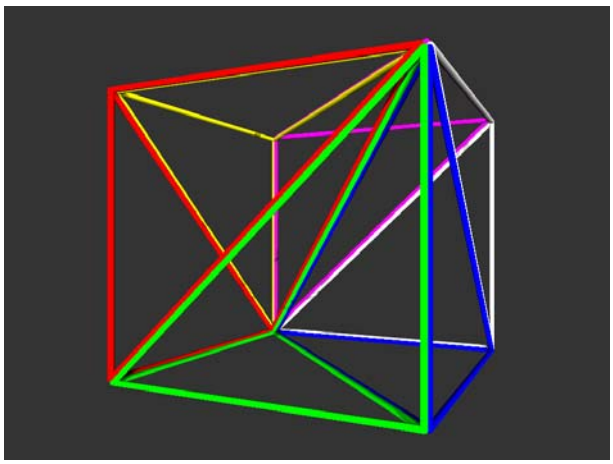

Fig. WP 5-13: Triangulation of a cube.

The advective flux F of the air mass through a surface A is computed from integral over the surface of the product of the relative velocity through the surface ***(v-c)*** and the air density ρ:

$$F = \int_A \rho(\vec{v} - \vec{c}) \cdot d\vec{n} \tag{5-1}$$

where ***n*** is the local normalvector on the surface. In this case, the given surface is the tropopause *P* as a function of space and time and defined as the locally lower surface of constant Ertel's potential vorticity (EPV = 3 PVU) or constant potential temperature (θ = 380 K).

The time rate of change of *P* following a trajectory is obtained from the Euler decomposition:

$$\frac{DP}{DT} = \dot{P} = \frac{\partial P}{\partial t} + \vec{v} \cdot \vec{\nabla} P \tag{5-2}$$

where ***v*** is the wind velocity. If *P* = const., the velocity on the right hand side is equal to the velocity of the tropopause (TP) ***c***:

$$0 = \frac{\partial P}{\partial t} + \vec{c} \cdot \vec{\nabla} P \tag{5-3}$$

where only the normal component of the TP velocity can be obtained from ***c*.** Since ***c*** cannot be determined directly from the model output, ***v*-*c*** is computed indirectly form the difference of the equations (5-2)-(5-3) and inserting into equation (5-1) leading:

$$F = \int_A \rho \frac{\dot{P}}{\left|\vec{\nabla} P\right|} dn \tag{5-4}$$

In (5-4) the production of *P* is either the production of the EPV, calculated from *Andrews, et al, 1987,* equation (3.1.5), or the net heating rate, quantities that all can be calculated from the primitive equation model KASIMA.

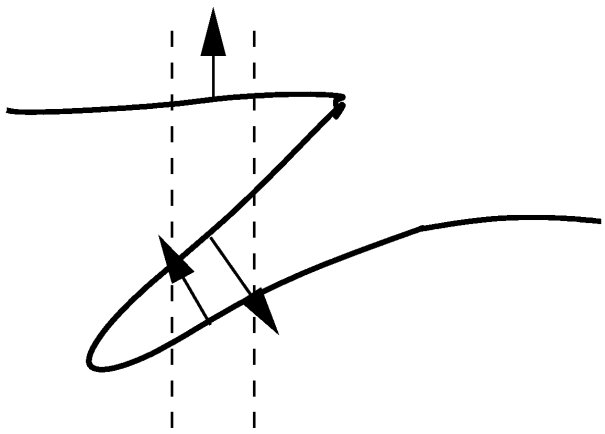

Fig. WP 5-14: Illustration of a tropopause fold.

This method for the analyses is equivalent to the method developed by *Wei (1987)*. He proposed a transformation using a function of the tropopause *P* as vertical co-ordinate which enables him to compute the inverse of grad *P* in equation 5-4 by the partial derivative with respect to *P*. This requires a vertically monotonic function of *P*, which is often violated in cases of significant cross tropopause mass fluxes (CTF) at the onset of frontal layers. With the implementation of *Sigmond et al., 2000,* who use a trajectory method to compute the production of *P*, the method is often used in applications. E.g. *Gettelman and Sobel (2000)* studied the CTF along a frontal layers. Compared to *Wei (1987)* this method uses the same basic concept but has numerically the advantage that all 3 spatial directions are treated in the same way and e.g. tropopause folds need no special handling and are resolved fully as long as the overall spatial resolution of the model is able to resolovle them. *Melone et al. (2003)*

performed a systematic intercomparison of different models to compute the CTF during a well defined cut off low in 1996.

In case a TP fold is resolved by the model grid, it is fully represented by the obtained set of triangles describing the TP. The gradient within each tetrahedral of *P* is defeined to allways point into the stratosphere. Therefore, if the production of *P* is positive, the flux obtained is always into the stratosphere, as indicated by the arrows in figure WP 5-14. A positive flux is hereafter also referred to as upward flux (into the stratosphere) independently of its geometric direction.

If horizontal maps of cross tropopause massflux (CTF) are shown (e.g. figure WP5-21) the total massflux through all triangles represented by the area of 1 horizontal grigpoint is related to the size of the horizontal area rather than the size of the sum of all triangles.

Case studies for evaluation

In order to evaluate the new method for computing CTF, some case studies are performed. They are selected from previously staudied cases published earlier in the literature. The physical reliability is also discussed from review articles e.g. *Palmén and Newton (1969)* and *Holton et al. (1995)*.

The upper tropospheric cut off low in June 1994 over the adriatic sea

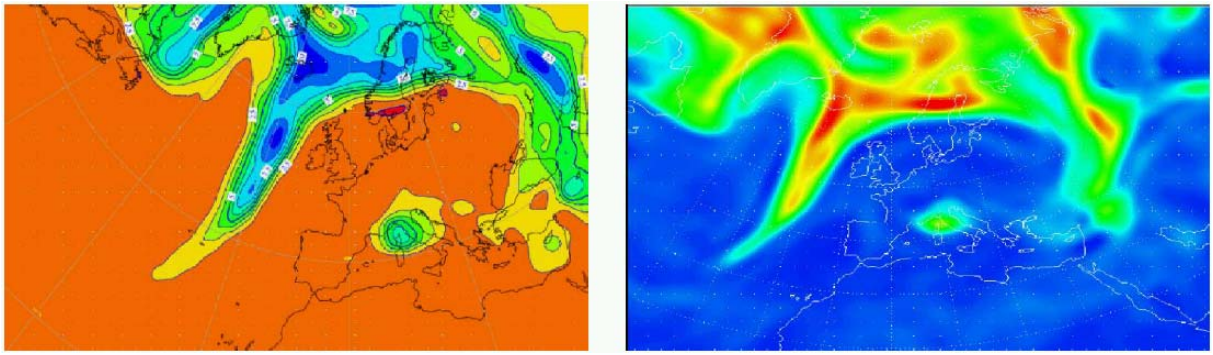

Fig. WP 5-15: Ertel's potential vorticity on the 330 K isentropic level, June 28, 1994. ECMWF ERA 40 data (left), KASIMA simulation (right).

Wirth and Egger (1999) (hereafter referred to as WE99) investigated an upper tropopspheric cut off cyclone and its impact on cross tropopause massflux (CTF) using several methods. This section describes in how far the CTF calculated with KASIMA and the triangulation method can confirm the results obtained previously by WE99.

Fig WP5-15 shows a comparison of the EPV obtained from the 40 year reanalyses data of the ECMWF (left) and obtained from the KASIMA model close to the tropopause at the 330 K isentropic level are considered. The cut-off low is visible in both figures as the maximum in the EPV over the Adriatic Sea. Moreover, the tongues of high EPV over the eastern Atlantic and Eastern Europe as analysed by ECMWF are well reproduced in KASIMA indicating a rather complex structure of the tropopause in these regions. Thus regarding this scale KASIMA prooves to yield reliable results.

Considering CTF processes, figure WP5-16 compares the production of the EPV as analysed by WE99 (left) and KASIMA (right). Both studies show a significant destruction of EPV of about 10 PVU/d and a weak production in the lower stratosphere. This again indicates that KASIMA is able to reproduce high derived physical quantities related to CTF in a reasonable way.

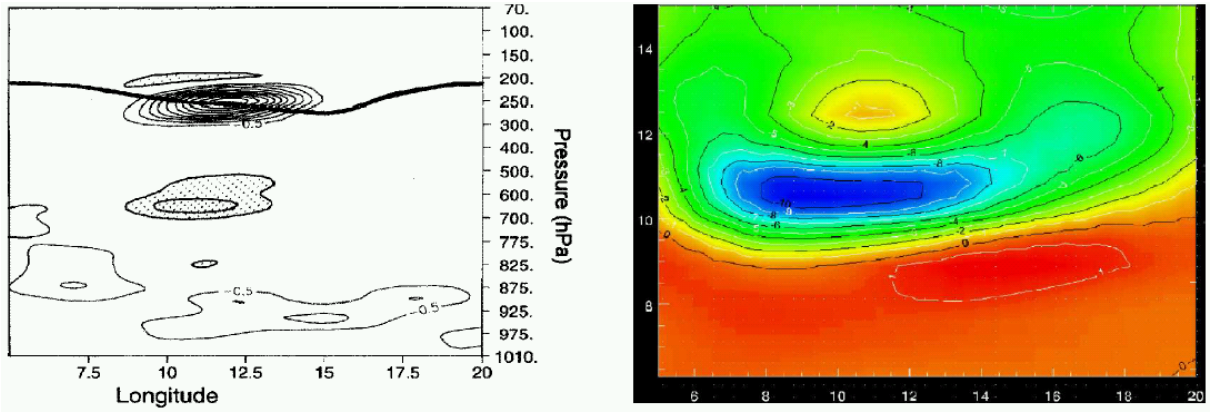

Fig. WP 5-16: Pressure- longitude cross section of the production of EPV (in PVU/d) in 45°N at June 28, 1994. Analyses of WE99 (left) and KASIMA (right). Please note that 200 hPa (left) = 11 km press. altitude (right).

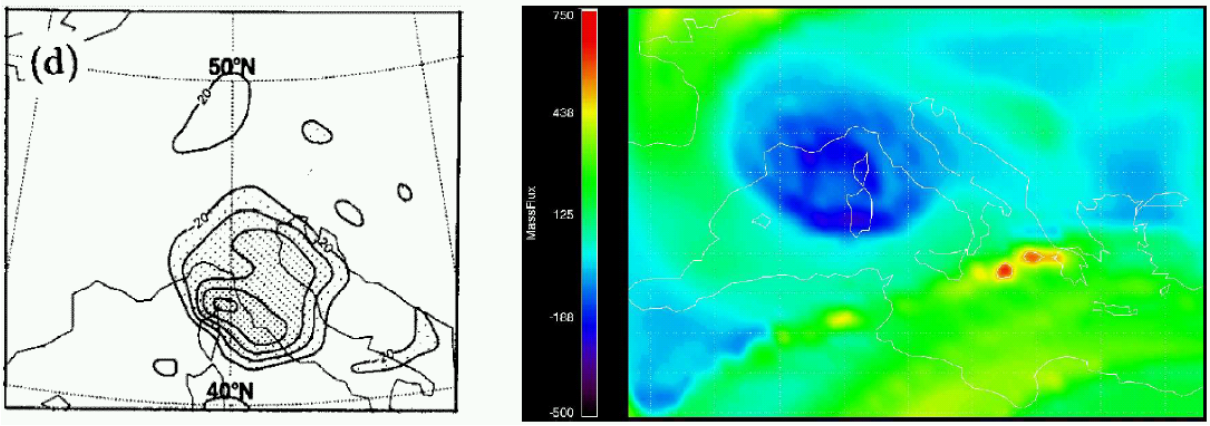

Fig. WP 5-17: Cross tropopause mass flux (CTF), June 28, 1994. Analyses of WE99 (left in hPa/d) and KASIMA (right in kg m^{-2} d^{-1}).

Correspondingly, the CTF computed by KASIMA (figure WP5-17, right) corresponds well to the previous study of WE99. The area of significant downward flux is larger in the KASIMA simulation whereas the absolut value of the downward flux of about 200 kg m^{-2} d^{-1} smaller than the value obtained by WE99 of about 50 hPa/d = 500 kg m^{-2} d^{-1} (1 hpa/d = 1g kg m^{-2} d^{-1} , where g is the earth's gravity acceleration from the hydrostatic equation)

Thus, regarding this case study, the setup of the KASIMA model and the triangulation method seems to be able to analyse the CTF processes of an upper tropospheric cut off cyclone reasonably.

Cross tropopause mass flux along a frontal zone

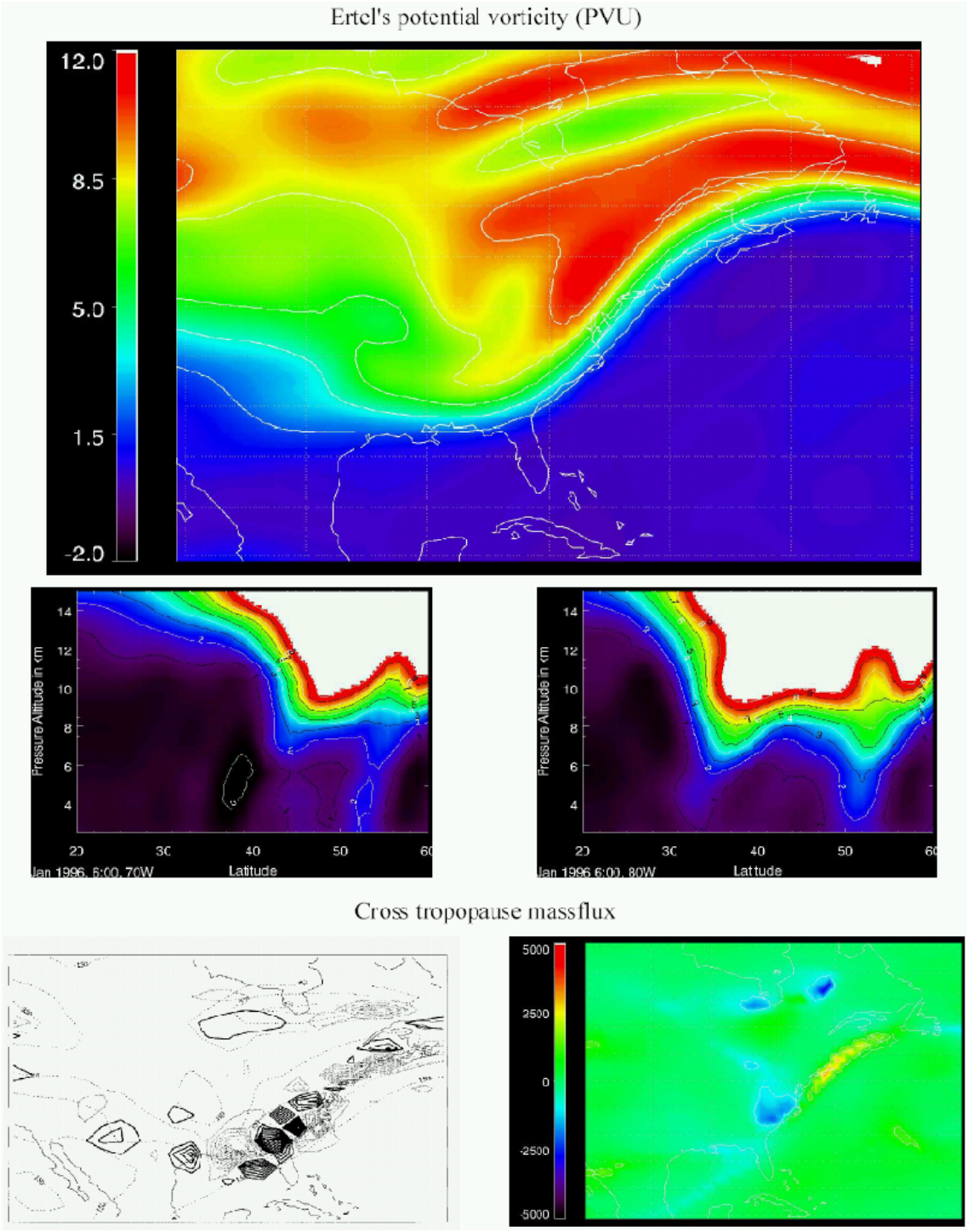

Fig. WP 5-18: Ertel's potential vorticity, January 4, 1996, KASIMA simulation. 330 K isentropic level (top), height-latitude cross section in 70°W (east of Cuba) and 80°W (Florida) (middle), and CTF taken from GS00 (bottom left) and KASIMA (bottom right in kg m^{-2} d^{-1}).

Gettelman and Sobel (2000) (hereafter referred to as GS00) investigated the CTF along a frontal layer over the east pacific to the West Atlantic in January 1996. Figure WP 5-18 shows the polar front along the east coast of the U.S.A. As the area of a strong gradient of the EPV as also visible in the height-latitude cross sections in 40°N, 70°W and 30°N, 80°W. The second maximum in about 50°N is related to an upper tropospheric low that is connected to a classical low south east of greenland and is therefore not regarded as a cut of cyclone as described in the last section *(DWD, 1996)*.

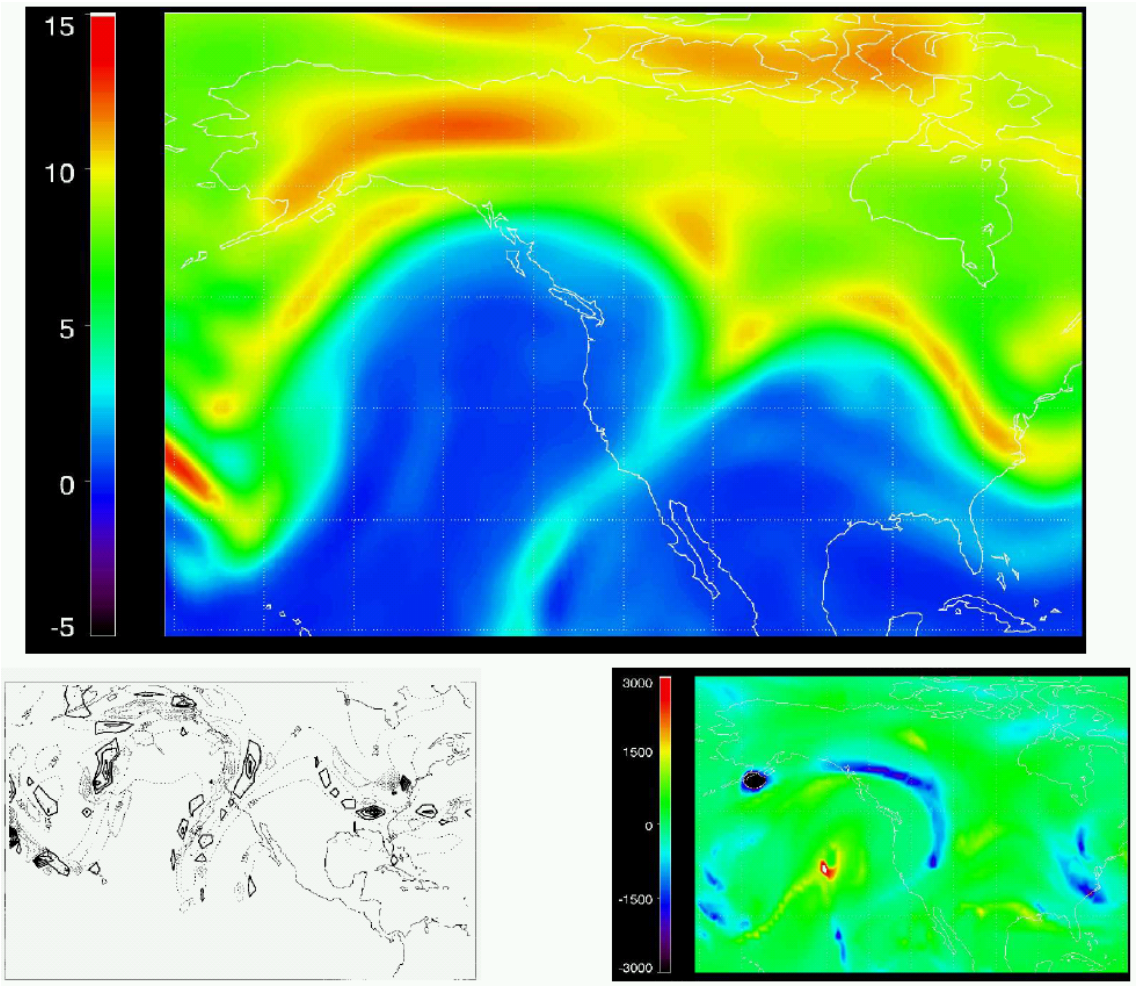

Fig. WP 5-19: Ertel's potential vorticity, January 10, 1996, KASIMA simulation. 330 K isentropic level (top), and CTF taken from GS00 (bottom left) and KASIMA (bottom right in kg m^{-2} d^{-1}).

The analyses of cross tropopause mass flux between GS00 and the KASIMA model differ considerably from each other. GS00 use the trajectory model of *Sigmond et al. (2000)* to compute the CTF. Whereas GS00 document an non systematic 2 way CTF north of Florida where the cold front is well pronounced, KASIMA computes a significant downward flux in this region, which coincides well with the general discussion in *Holton et al. (1995).*

This result becomes even more significant at January 10 (figure WP5-19), when a frontal zone is observed over the western part of the U.S.A. Building an arc over the eastern pacific ocean. GS00 again compute a non systematic CTF in both directions whereas KASIMA computes a systematic downward flux into the troposphere.

From this case study it might be concluded that KASIMA computes a CTF which reproduces the physical model of a downward flux being caused by

1. transport of high EPV (stratospheric) air into middle tropospheric heights within the frontal layer, and
2. mix the frontal air adiabatically into the troposphere in later stages of the frontogenesis.

One possible reason of the appearent advantage of the KASIMA model for this case is that the method of *Wei (1987)* of transforming the equations into a system where the EPV is the vertical co-ordinate implies that the EPV is a monotonic function with altitude. Moreover, the method of *Sigmond et al. (2000)* is crucial regarding the amount of mass and the size of the tropopause surface represented by each trajectory.

Cross tropopause climatology

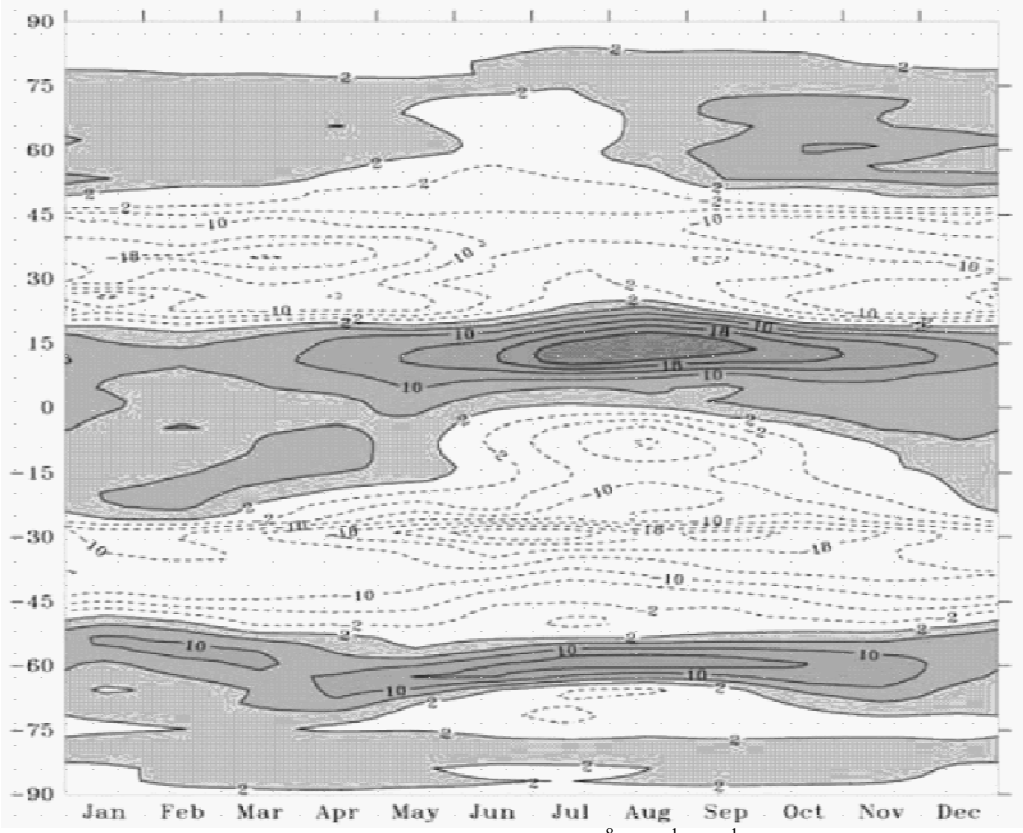

Fig. WP 5-20: zonal mean time-latitude cross section of CTF (10^8 kg s^{-1} deg^{-1}) from *James et al., 2003.*

As a reference, figure WP 5-20 shows the CTF as a zonal mean sesonal cycle *(James et al., 2003).* A number of aspects of this picture can be anticipated from a knowledge of the general circulation, such as the mean net upward flux above the inter-tropical convergence zone (ITCZ), especially during the northern summer when the ITCZ shifts northwards over regions where a greater percentage of land surface (than further south) induces more intense convective cells. Over the subtropics and midlatitudes up to about 50° N and 50° S, respectively, a mean net downward flux is seen, where midlatitude troughs extend towards the subtropics. Polewards of these regions, by contrast, a mean net upward flux is seen, typically associated with warm conveyor belts, especially those which stream polewards and westwards of blocking anticyclones.

Based on the results of the case studies which show a good agreement of the KASIMA results with other studies or with expected results from the knowledge of the general circulation, a comparison to the results of *James et al. (2003)* is done with KASIMA (figures WP 5-21, WP 5-22). Here a 10 year model run is performed with data output every 12 hours which is then statistically evaluated. Figure WP5-21 shows time-latitude cross sections of the CTF, the tropopause (TP) height, its temperature and the criterion applied to diagnose the TP. For each timestep, the criterion gets the value of 1 (0) indicating, the TP is evaluated at this gridpoint from the potential temperature (EPV). The figures are taken from zonal and monthly mean data. The bottom panel shows the CTF for a 3-year period only, in order to better resolve the seasonal depenencies. By accident, the data of 1962 was lost, therefore this year appears as a straight area in the figures.

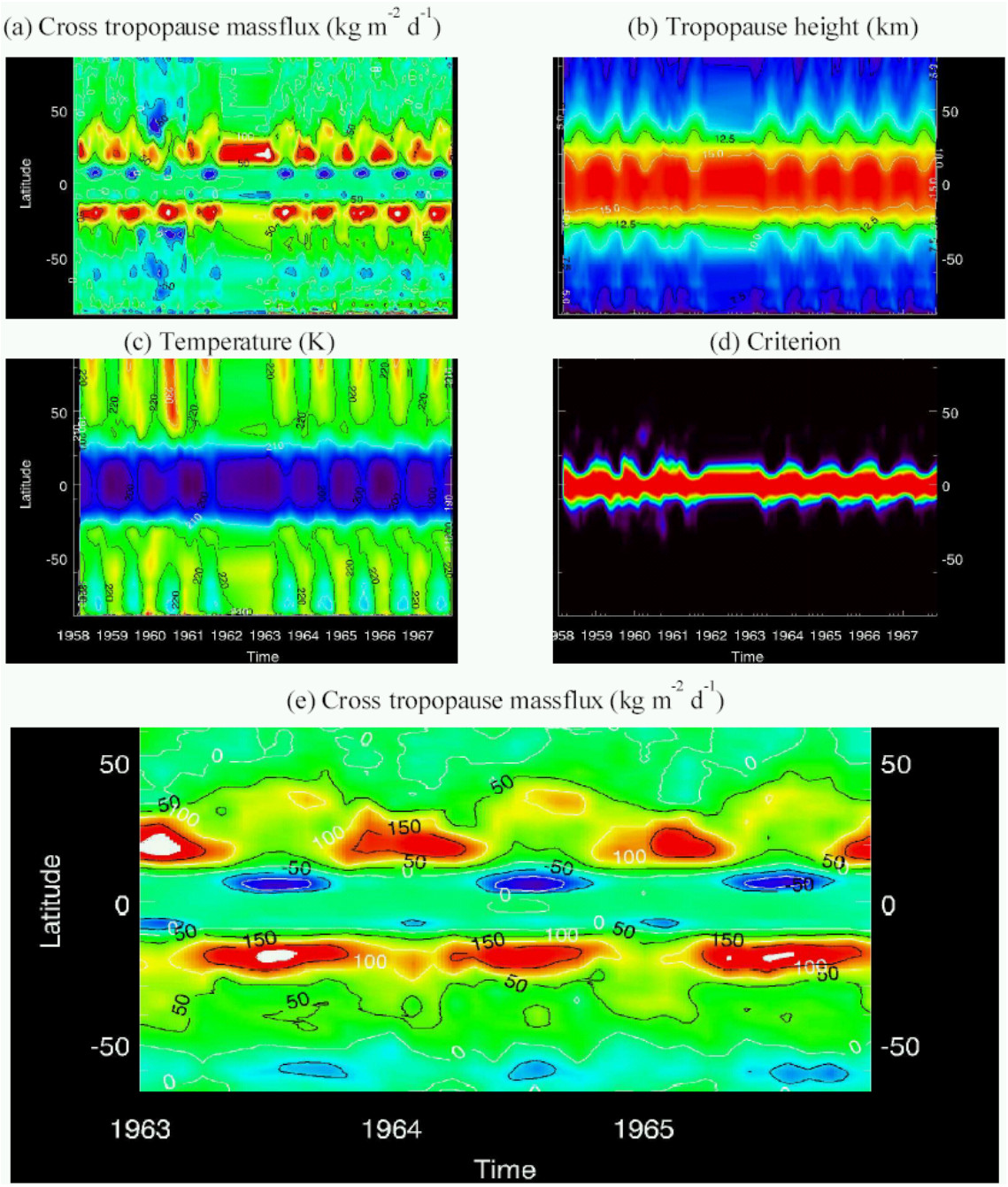

Fig. WP 5-21: Zonal mean time latitude cross sections of tropopause analyses, KASIMA.

Whereas the overall structure of the TP reflects well the structure of the TP, i.e., the TP is cold and heigh in the tropics and has a seasonal cycle in the extratropics being heigh and warm in the summer hemispheres, the CTF anlysed here shows significant differences to other results. Whereas in northern hemisphere extratropics the KASIMA result of about 10 kg m^{-2} d^{-1} ($\approx$ 5 10^{8} kg deg^{-1} s^{-1} in 60° latitude) agree well with the resuts of *James et al. (2003)*, this study shows an almost symmentric downward flux in the southern hemisphere extratropics.

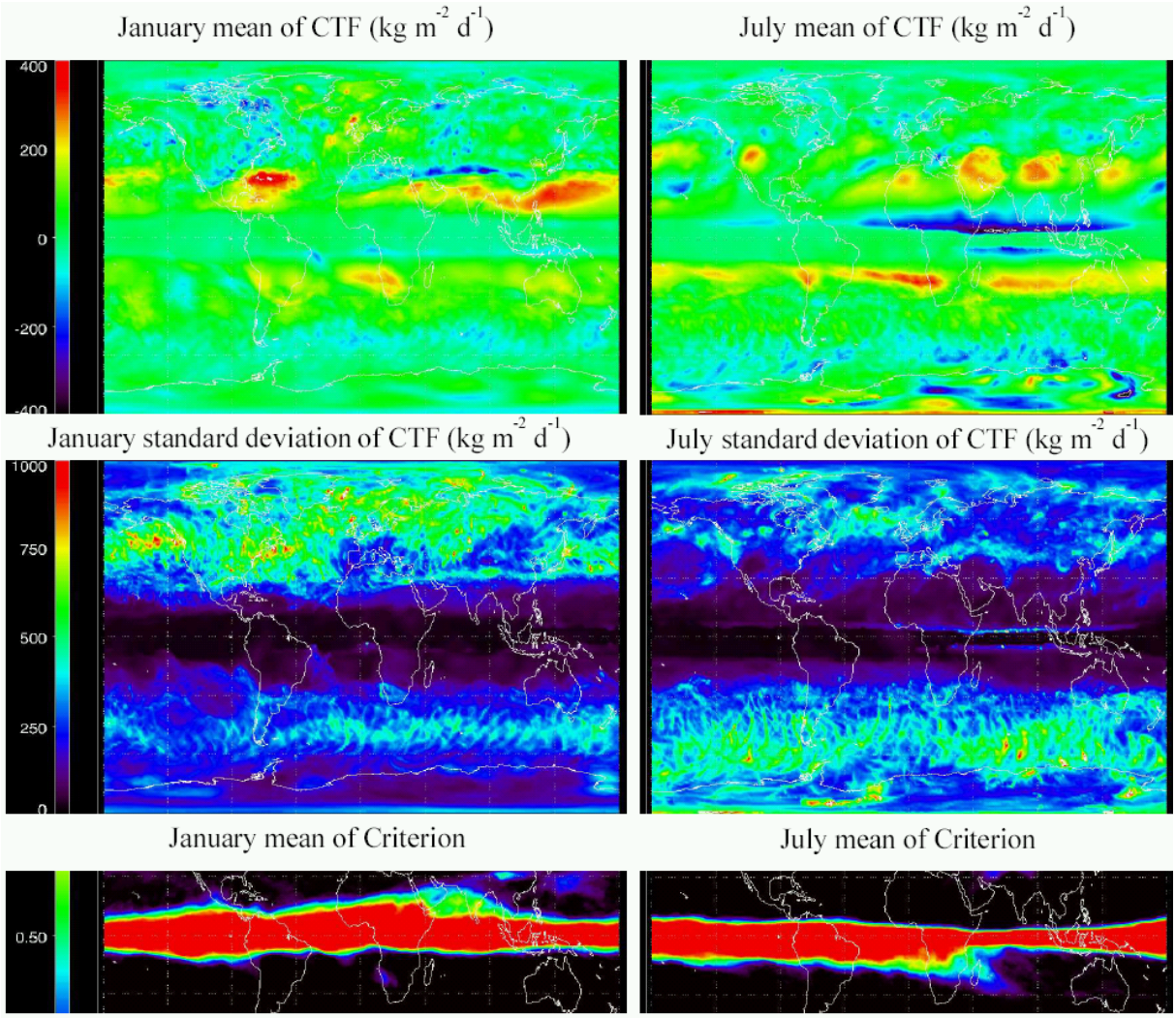

Fig. WP 5-22: Statistics of Januery 1964 (left) and July 1964 (right) of cross tropopause mass flux.

The most significant differences occur however in the subtropics and tropics. Unlike this study (see section *development of an analyses scheme)* most studies like *James et al. (2003)* and *Gettelman and Sobel (2000)* define the TP equatorwards of mostly 20° either by means of the themal TP or by a critical value of the potential temperature. From figure WP5-21 it is seen, that the evaluation of the TP from the potential temperature in confined to a very tiny band around the equator. Thus, the upward CTF as seen in figure WP5-21 a and e in about 20° latitude each winter season of more than 150 kg m^{-2} d^{-1} is clearly obtained from an EPV TP. In these latitudes classical studies (e.g. *James et al. (2003)* and references therein) show upward fluxes especially in northern hemisphere summer, when the inner tropical convergence zone is shifted over the Asian continent.

Within the tropics, especially where the TP is evaluated from potential temperature, the calculated CTF is considerable weaker and mostly downward in this study. The strongest fluxes occur in July at about 10°N. However, as can be seen from figure WP 5-22, right cloumn, this downward flux takes place along a small latitude band around 10°N from Africa south of India to Indonesia. From the criterion, this region is the southmost part of the northern hemisphere, where the TP is evaluated mostly from the EPV instead of the potential temperature, as would be expected. This very tiny band together with its mirror is also identified as a region with a peak in the variability of the fluxes, which has the same the order of magnitude of 500 kg m^{-2} d^{-1} than the fluxes, in an ovarall area of weak variability in the entire tropics (figure WP 5-22, 2nd row).

As is already seen from figure WP 5-21, the most significant deviations from classical CTF analyses occur in the winter subtropical areas, where considerable upward flux is analysed in this study. From figure WP5-22 the areas of upward flux can be associated to regions where quasi stationary high pressure areas are found in the upper troposphere (figure WP 5-23, top) in the area of the subtropical jet stream, already reported e.g. by *Palmen and Newton (1969)*.

Discussion and Conclusion

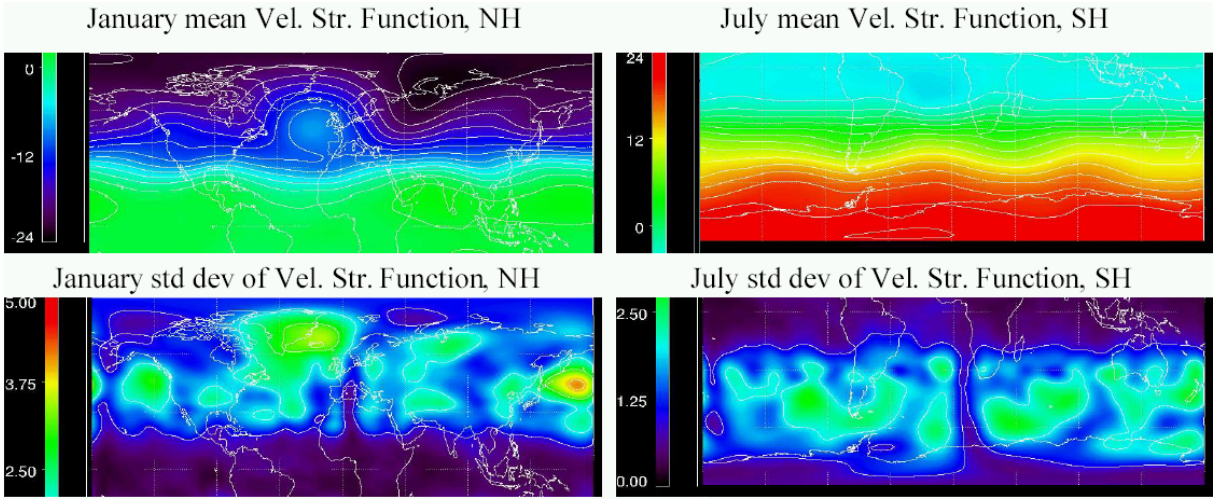

Fig. WP 5-23: Statistics of Januery 1964 (left) and July 1964 (right) of the velocity stream function, 200 hPa, winter hemispheres.

The case studies dealing with an upper tropospheric cut-off cyclone and a frontal layer simulate CTF processes according to actual meteorologigal models, as recently reviewed by *Holton et al. (1995)*:

- WE99 explained the downward transport at the end of the cut-of cylone with heavy rainfall, that removes latent heat irreversable out of the atmosphere. Thus, a vertical gradient of the net heating is generated by an almost adiabatic lower stratosphere and the heating of the upper troposphere which in turn acts as a net destruction of EPV in that region. Therefore, surfaces of constant EPV and therefore the TP raise impliing a downward massflux through the tropopause into the tropopsphere.
- CTF due to a frontal layer should be downward, because during the frontogenesis stratospheric air with high EPV is transported along the frontal layer downward and in later stages irreversibly mixed with surrounding tropospheric air. Thus, its EPV reduces to tropospheric values indicating the downward mass flux *(Holton, et al., 1995)*.

In the subtropics and tropical latitudes, this model seems to fail:

- Around the subtropical jet this model calculates the most significant upward massflux in both winter hemispheres, whereas
- The expected upward massflux in the tropics caused ba heavy convection in the ITCZ is not reproduced. In contrast: In the tiny region around the equator where the TP is determined by θ only a weak vertical massflux is simulated.

Some possible reasons/explanations for these results can be summarized as the following hypotheses:

- In contrast to the mid-latitude Ferrel cell, which is wave driven and is therefore not associated with a significant transport of mass, the trade wind circulation is a thermal direct ciculation, which effectively transports mass, heat, and momentum. (e.g. *Andrews and McIntyre, 1976, Dunkerton, 1978).* Assuming the poleward mass transport is conservative, air with low tropical EPV is

advected poleward in the upper troposphere feeding in the subtropical horse latitudes due to the advection of earth vorticity the subtropical jet and forming the upper tropospheric heights. In these latitudes the tropical air mixes with mid-latitude air of heigh EPV, which leads to a net production of EPV and thus to an upward mass flux through the tropopause.

- In the tropics, the choosen 380 K isentropic surface might be too high not reached by the convection, which is supposed to cause via latent heat release an upward massflux through the TP. On the other hand, this model uses the results of the global analyses model of the ECMWF as input especially for the heating rates via the described nudging mechanism. Since the effects of convection processes in the ITCZ are parameterized the ECMWF model, a non-realistic implementation there may lead to a failure in KASIMA. Tests of these hypotheses, especially a variation in the critical value of θ for the TP, are however outside the scope of this staudy.

As a conclusion, this study shows that the applied scheme to quantitatively analyse the tropopause is a promising tool that does not only confirm existing models for STE processes but also leaves some open questions. The most remarkalbe is: If the main upward flux occurs in Winter subtropical regions, what is the exact way of the air from the troposphere into the stratosphere. Answeres to this question are of immediate importance for the stratospheric ozone problem, which is partly due to the transport of the source gases through the tropopause inteo the stratosphere

Contribution of IMK-MIPAS

MIPAS on ENVISAT was launched on 1 March 2002. It provides global spectral measurements from about 6 km altitude up to the mesosphere from which volume mixing ratio profiles of water vapor and temperature can be retrieved. At IMK a scientific data processor of higher sophistication has been developed. It is based on an optimal estimation scheme which supports both probabilistic and non-probabilistic covariance matrices for the regularization of the retrieval problem. Full retrieval diagnostics in terms of covariance matrices of the retrieval results, averaging kernel matrices, measure of the vertical resolution etc. is also provided. The development work for the water vapor and temperature retrievals has focussed - as part of the overall development of this processor- on the optimization and fine-tuning of the retrieval of non-standard observations for which the routine processing by ESA will most probably not be optimized. During the year 2001 we concentrated on the development of the retrieval approach for water vapor in the tropical UTLS from the standard observation scenario (covering 6 to 68 km altitude in 3 or 5 km steps) and the specific UTLS observation scenario S2 (covering 5 to 20 km in 1.5 km steps and 20 to 40 km in 5 km steps), for both based on simulated data.

Development of retrieval methods

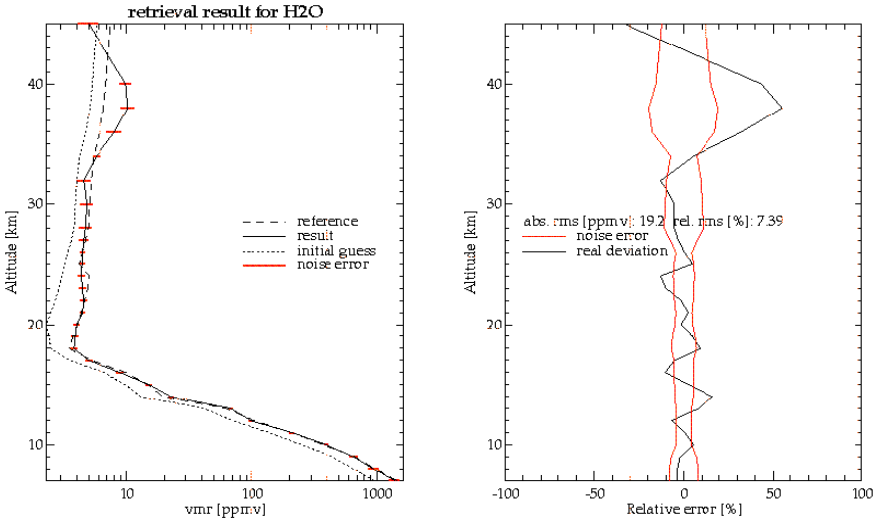

Fig. WP 5-24: Test retrieval based on synthetic data for the tropical UTLS region and the specific UT/LS observation scenario S2 (covering 5 to 20 km in 1.5 km steps and 20 to 40 km in 5 km steps). Left panel: Retrieved profile (solid line), reference profile (dashed line), initial guess (dotted line) and error bars due to measurement noise; right panel:deviation from the reference profile compared to the estimated standard deviation.

For the tropical UT/LS region, the retrieval approach for water vapor has been developed by an appropriate selection of spectral microwindows, and by fine-tuning the regularization of the retrieval via test retrievals using synthetic data.

Fig. WP 5-24 shows the result of a test retrieval based on synthetic data for the tropical UT/LS region and the specific UT/LS observation scenario (covering 5 to 40 km in 1.5 km steps). Water vapor and temperature in the altitude range of the measurement were the parameters to be retrieved. The reference spectra had been perturbed by measurement noise according to the MIPAS/ENVISAT specification. All other potentially perturbing parameters (interfering gases etc.) have been assumed to be exactly known. The test retrievals showed that the water vapor mixing ratio profile in the altitude range of the observations can be reconstructed very well; the water vapor volume mixing ratio can be retrieved to an uncertainty of about 10 % for the given conditions in the tropopause regions, and the hygropause can very well be resolved.

First retrievals based on real data

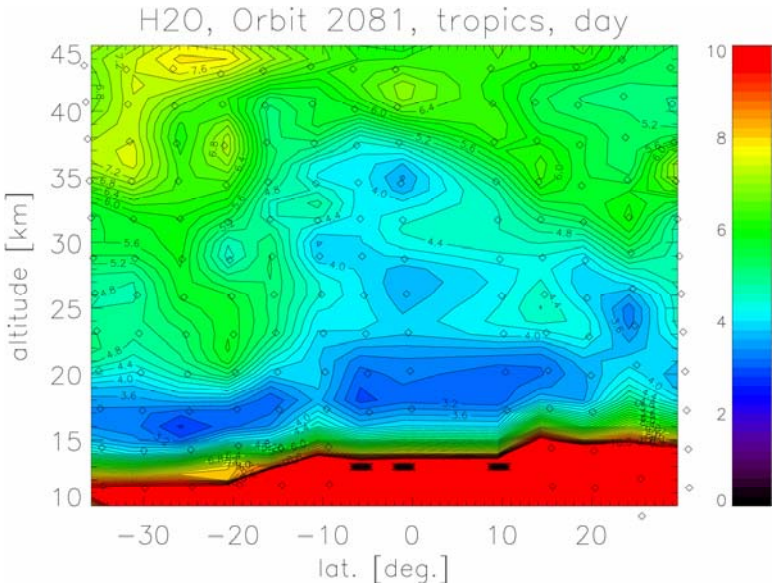

Fig. WP 5-25: Water vapour volume mixing ratio (VMR in ppmv) distribution as retrieved along part of orbit no. 2081 (measured on 24 July 2002 during day time) for the tropics west of the western African coast. Values equal or above 10 ppmv as present in the troposphere are shown as red areas. The diamonds mark the tangent altitudes of spectral data used in the retrieval. Gaps indicate that spectral data have been omitted due to optically thick clouds (up to the tropopause) or other reasons (one scan at about +5° latitude is missing).

During the commissioning phase several groups were given the opportunity by providing a limited amount of spectral data sets to test their data processing systems and to contribute to calibration/validation issues. As part of our activity within KODYACS, our retrieval system for water vapor volume mixing ratio and temperature was applied to these data, and the approach was tested in detail and refined where necessary. Three orbits of data measured on 24 July 2002 (orbit no. 2081 to 2083) were used for the tests. Based on the derived tangent altitudes and temperatures water vapor test retrievals with various choices for the retrieval control parameters (microwindow selection, regularization, exclusion of cloud-contaminated measurements, etc.) were performed. Part of one derived water vapor volume mixing ratio fields for orbit no. 2081 covering the tropics and subtropics is shown in Fig. WP 5-25. Meaningful data, i.e. with the information from the measurement dominating the retrieval results, can be obtained between the upper troposphere (3 - 5 km below the hygropause) and about 55 km. The varying altitude of the hygropause along the orbit can clearly be seen. Three individual profiles retrieved from orbit no. 2081, scans no 5, 13, and 18, are shown in Fig. WP5-26 as typical examples of the profile shapes obtained for polar summer, northern midlatitudinal and tropical conditions.

From these results we concluded that our data processing system had passed the functionality tests. Next steps were further optimization of the retrieval control parameters, and, as the main activity, derivation of water vapor distributions from observations in the standard and UTLS observation mode.

Measurements of water vapour in the tropopause region with MIPAS/ENVISAT

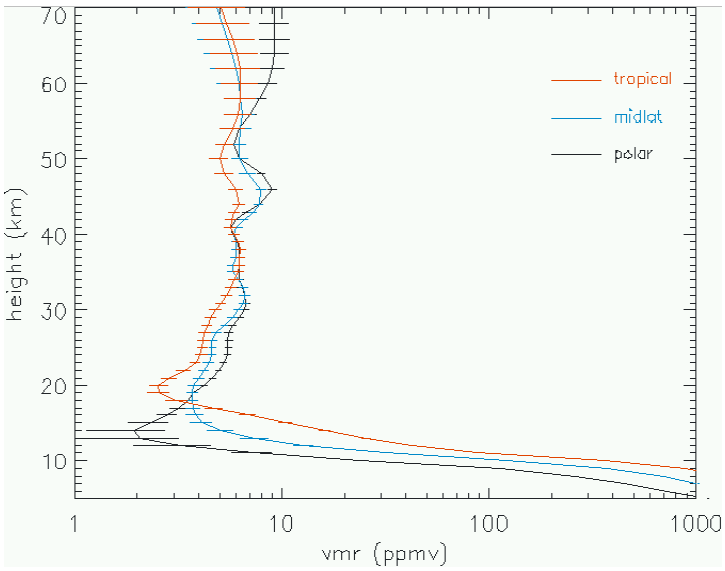

Fig. WP 5-26: Three individual profiles retrieved from orbit no. 2081, scan no. 5 (polar winter), 13 (midlat), and 18 (tropical), together with their random errors. They differ by the altitudes of the hygropause and minimum VMR values reached there.

In June 2003 measurements were taken in non-standard observation modes dedicated to specific scientific questions. Among those, several orbits were taken in the so-called UTLS (S2) mode which shall provide improved measurements of parameters in the upper troposphere and lower stratosphere. The altitude range between 5 and 20 km is scanned with altitude steps of 1.5 km (instead of 3 km in the standard observation mode). From observations in the S2 mode water vapor distributions along the orbit were retrieved, and the retrievals were compared to those of the standard observation mode, as well as analyzed in further detail (see Fig. WP 5-27).

The averaging kernel matrices (Fig. WP5-27, middle row) are in particular useful, since the vertical resolution and the impact of a priori information on the retrieval can be assessed from its values. The values along the rows of the averaging kernel show from which altitude of the atmosphere the information for the retrieval altitude of the respective row comes. The column shows in which altitudes the retrieval reacts on a delta perturbation in the atmosphere at the respective altitude of the column. The half width of either the rows or the columns of the averaging kernel matrix are a measure of the vertical resolution of the retrieval. For the UTLS (S2) mode (see middle right panel in Fig. WP5-27), information on the atmosphere can be gained down to appr. 6 km, which is 1.5 to 2 km farther down than for the standard observation mode. The vertical resolution is around 4.5 km in the lower stratosphere for the standard observation mode (see lower left panel in Fig. WP 5-27), while it is better than 3 km for the UTLS mode. The vertical resolution will be improved further in future when re-processed level-1b data will become available for which a currently existing problem in the gain calibration procedure will be resolved. In the current level-1b data version inappropriate gain calibration produces oscillations in the vertical radiance profiles which lead to similar and even amplified oscillations in the vmr profiles of certain species, among those also H_2O. In our current retrieval set-up, these are suppressed by application of stronger regularisation in the vertical domain which, however, results in somewhat reduced vertical resolution in the retrieval.

In the last row of Fig. WP 5-27 the total error budgets for the standard observation mode (left panel) and the UTLS mode are compared. The UTLS modes provides accuracy of better than 5 % in the tropopause region, while for the standard observation mode accuracy of around 10 % in the lower stratosphere and around 20 % in the tropopause region can be reached.

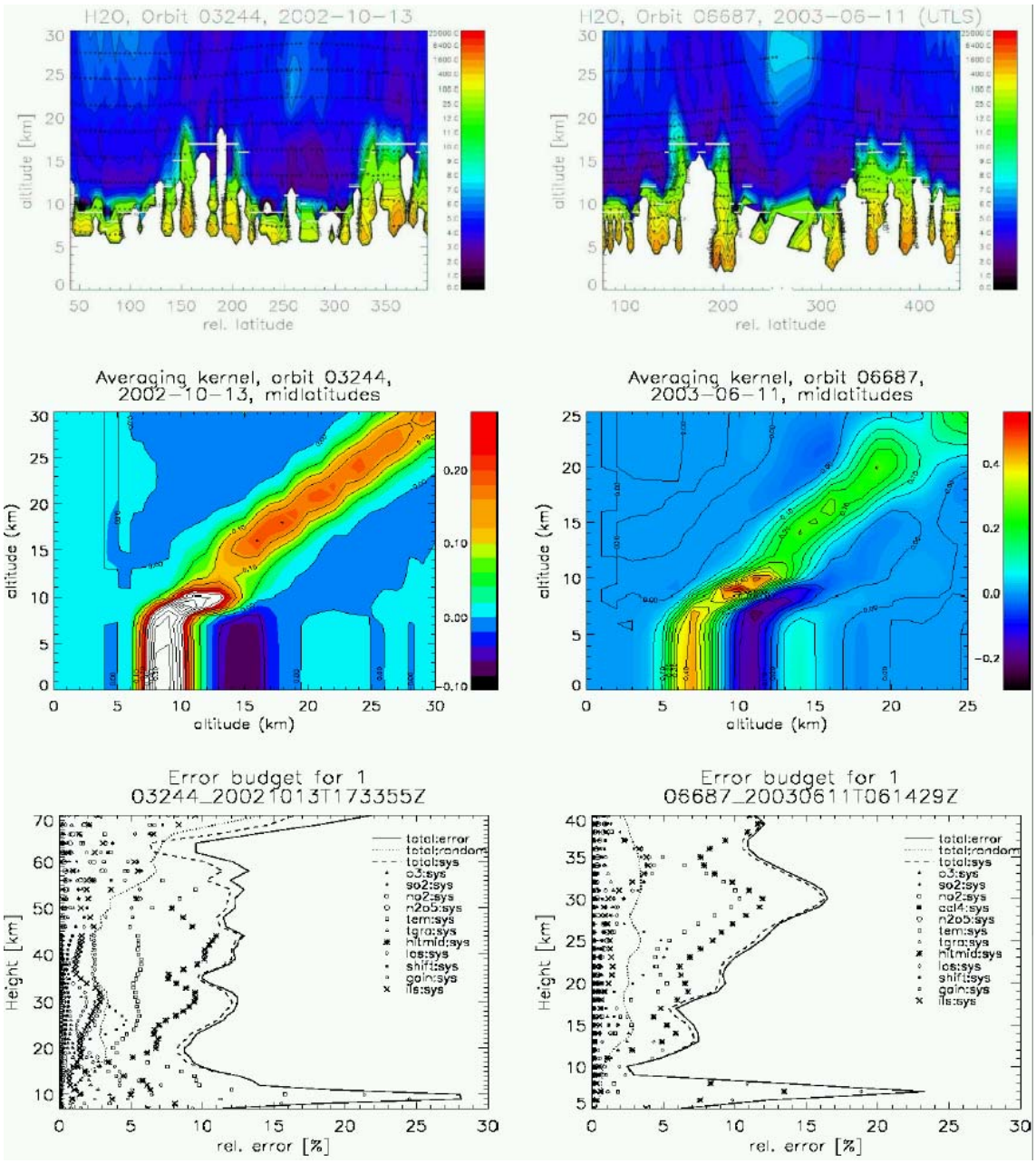

Fig. WP 5-27: Comparison of standard observation mode (left column) and UTLS (S2) observation mode (right column). The upper row shows the water vapour distributions along an orbit of the respective observation mode. The middle row provides the averaging kernel matrices (for explanation, see text). The lower row compares the total error budget including all random and systematic errors for the two observation modes.

In summary, the finer scanning step width results in an improved vertical resolution and an altitude range extended further down into the troposphere. Analysis of MIPAS scans which are cloud-free in the relevant altitude range show that the quality of the retrieved data is improved in terms of accuracy and vertical resolution

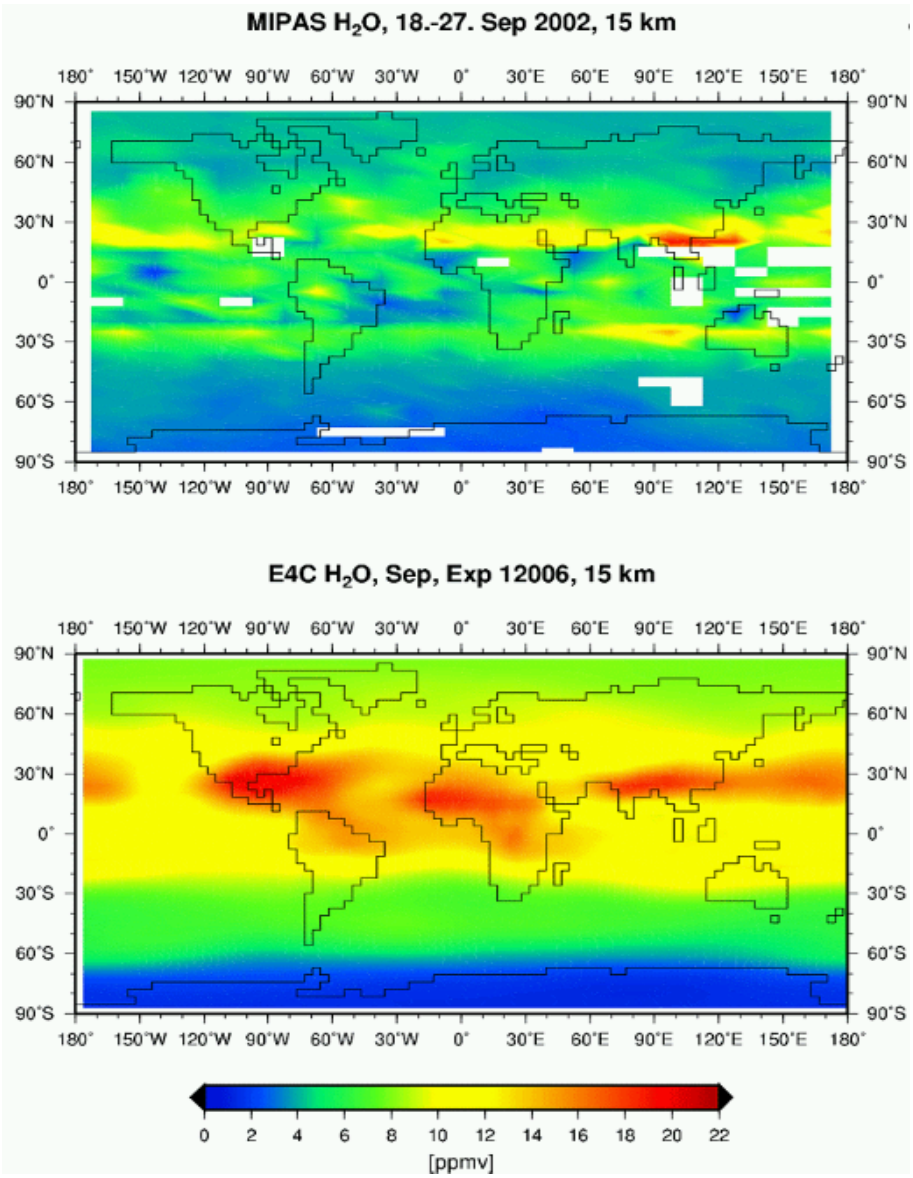

Fig. WP 5-28: Global mean water vapour distribution from MIPAS September 2002 measurements averaged for bins of 5° latitude x 15° longitude at an altitude of 15 km (upper panel), compared to DLR CCM run (lower panel). The increased water vapour vmr around 25° N/S is clearly visible in the MIPAS water vapour distribution, most pronounced over East Asia.

Although still in the commissioning phase ESA released MIPAS/ENVISAT data for scientific use covering the period of the Antarctic major warming in September/October 2002. At IMK/University of Karlsruhe global data sets on the distribution of a number of trace species were retrieved for the observation days 18 to 27 September and 11 to 13 October 2002. In particular, water vapour distributions covering the upper troposphere to the stratopause were retrieved for these days. The retrieved H_2O distributions along the orbits and the resulting zonal averages demonstrate the high quality of the MIPAS measurements for the lower and middle stratosphere. Besides expected structures like a high and dry hygropause in the tropics, the dehydration in the south polar vortex which took place during the austral winter could be demonstrated by means of correlations between methane and water vapour. An interesting feature of these distributions is a region of increased water vapour mixing ratios (vmr) in the subtropics around 25° latitude and an altitude rage of 15 to 18 km. The vmr are higher there than in the tropics at similar altitudes. This hints towards upward transport processes of moist tropospheric air in the subtropics, while air entering the stratosphere over the tropics seems to be much dryer. This observed feature in the MIPAS water vapour distribution will be analysed in more detail in near future.

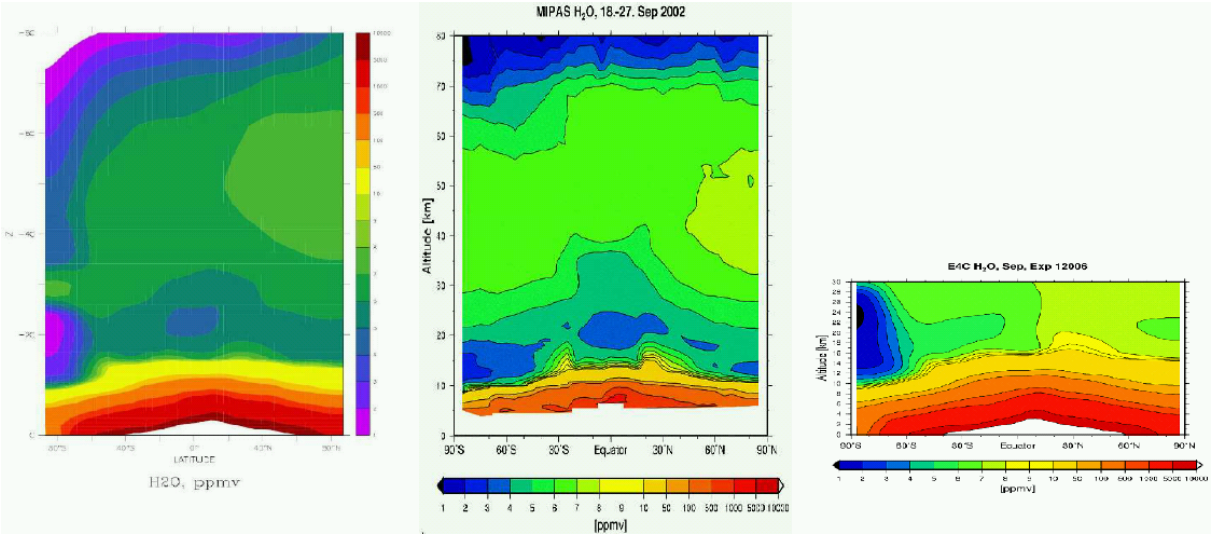

Fig. WP 5-29: Water vapour mixing ratio derived from MAECHAM4/CHEM transient simulation, September 1998 (left; courtesy C. Brühl), MIPAS/ENVISAT for September 2002 (middle), and E39/C time-slice simulation "2000", 10-year climatology (right; courtesy M. Dameris).

From the measured profiles of the September 2002 period zonal averages in terms of a latitude-altitude cross-section, as well as a global mean distribution averaged over bins of 5^{o} latitude x 15^{o} longitude was derived. The September 2002 mean water vapour distribution at an altitude of 15 km is given in Fig. WP5-28 and is compared to the results from CCM runs performed at DLR (M. Dameris, pers. communication).

Fig. WP 5-29 compares the latitude-altitude cross-section for water vapour from MIPAS September 2002 observations with those produced by two different ECHAM runs (C. Brühl, M. Dameris, pers. communication, 2004). Main structures of the global distribution, like a dry area just above the tropical tropopause, dry lower stratosphere and mesosphere over the winter pole, and the stratospheric vmr maximum in the middle stratosphere over the summer pole, are visible in all three distributions. Particularly interesting, however, are the areas of increased water vapour vmrs in the subtropical tropopause region. They occur also in both model runs and are, similar to MIPAS data, more pronounced in the Northern hemisphere. These structures have not been observed so far with comparable clarity, for example from HALOE data.

Contribution of MPI-C

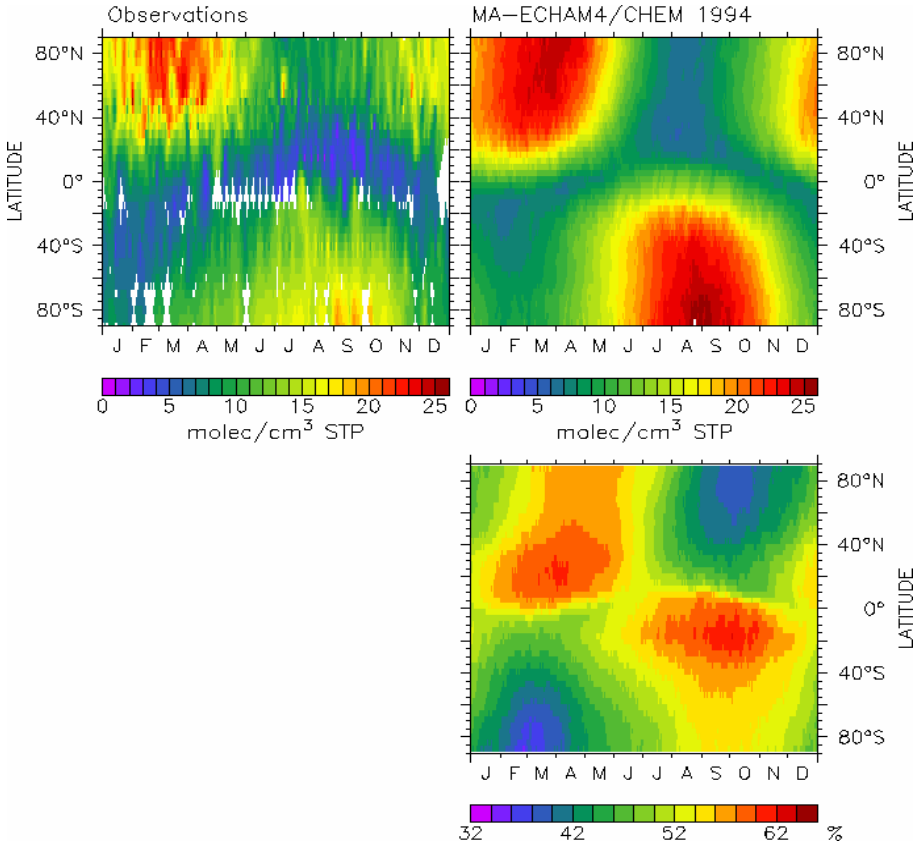

Figure WP 5-30: Left: Zonal average climatology of cosmogenic ^{14}CO compiled from total ^{14}CO observations at the surface level: The biogenic (secondary) ^{14}CO has been estimated and subtracted from the observations of atmospheric ^{14}CO. The cosmogenic contribution is in molec/cm3 STP, standardized to the average solar conditions during the period 1955 to 1988. The climatology shows a clear asymmetry between the NH and the SH. Right: Zonal average ^{14}CO mass mixing ratio at the surface level calculated with the GCM for the year 1994 (upper), and corresponding fraction (in %) of ^{14}CO originating from the stratosphere (lower).

As a diagnostic for transport from stratosphere to troposphere ^{14}CO, which is produced by cosmic rays in the high latitude lower stratosphere and upper troposphere, is used (Jöckel et al., 2002). To separate the source regions, two ^{14}CO tracers are computed during the transient simulation with MAECHAM4/CHEM. The mass mixing ratios are scaled to an average global average ^{14}CO production rate of 1.76 molec/cm^{2}s, corresponding to the time average used for the climatology in Figure WP5-30, left. The calculations have been done with climatological OH (Spivakowski) to separate effects of transport across the tropopause from effects of model OH in the troposphere and its changes with time.

Transport from stratosphere to troposphere of the stratospheric ^{14}CO-tracer is overestimated by about 60% in the Southern Hemisphere (winter/spring) and 35% in the Northern Hemisphere. This holds for the whole timeseries without significant trend, there are however some variations related to the interannual variability of the polar vortices. With 'online' OH results get better in the Northern Hemisphere and worse in the Southern Hemisphere. The overestimate of downward transport is partially related to model resolution and discussed in detail in Steil et al (2003).

Joint contribution of IMK-KASIMA and DLR

Streamers in the middle stratosphere

The transport of tropical air masses to mid and high latitudes is characterised by high N_2O and low ozone values compared to undisturbed mid-latitude values. Those so called *streamers* reach from lower into extra-tropical latitudes. Streamers can be seen in the horizontal gradient of an N_2O tracer field at a certain pressure level. N_2O usually decreases from the equator towards the pole in both hemispheres, which means that the N_2O gradient is in general negative in the northern and positive in the southern hemisphere. A streamer can therefore be defined by a change of sign in the N_2O gradient (see figure WP5-31). If irreversible mixing occurs, streamer events significantly contribute to the transfer of tropical air masses to mid-latitudes which is also an exchange of upper tropospheric and stratospheric air. A meridional streamer criterion has been newly formulated and has been applied to derive a climatology of streamer events in the altitude region between 21 and 25 km, employing the chemical-transport model KASIMA, which is driven by ECMWF re-analyses (ERA) and operational analyses. For the first time, the seasonal and the geographical distribution of streamer frequencies has been determined on the basis of 9 years of observations (1990 to 1998).

It has been further used for the validation of a streamer climatology which has been established in the same way employing data of a multi-year simulation with the coupled chemistry-climate model ECHAM4.L39(DLR)/CHEM (E39/C). It turned out that both climatologies are qualitatively in fair agreement, in particular in the northern hemisphere, where much higher streamer frequencies are found in winter than in summer. In the southern hemisphere, KASIMA analyses indicate strongest streamer activity in September (figure WP5-32). E39/C streamer frequencies clearly offer an offset from June to October, pointing to model deficiencies with respect to tropospheric dynamics. KASIMA and E39/C results fairly agree from November to May. Some of the findings give strong indications that the streamer events found in the altitude region between 21 and 25 km are mainly forced from the troposphere and are not directly related to the dynamics of the stratosphere, in particular not to the dynamics of the polar vortex.

Sensitivity experiments with E39/C have been used to assess the impact of streamers on the ozone budget at mid-latitudes. As found in recent investigations, an altitude dependency of the mass of streamers has been indicated by E39/C results. A simple model assessment shows that the effects of streamers on the mid-latitude ozone distribution have much larger impacts in the lower stratosphere than in the middle stratosphere. The decrease of ozone at around 25 km is of the order of less than 5% whereas at around 15 km it can reach 80%. Therefore, it is obvious that a realistic simulation of streamers (amount, distribution, seasonal cycle) in CCMs is necessary to calculate the ozone budget at mid-latitudes in a realistic way. The current study indicates that this requires an adequate representation of horizontal transport processes.

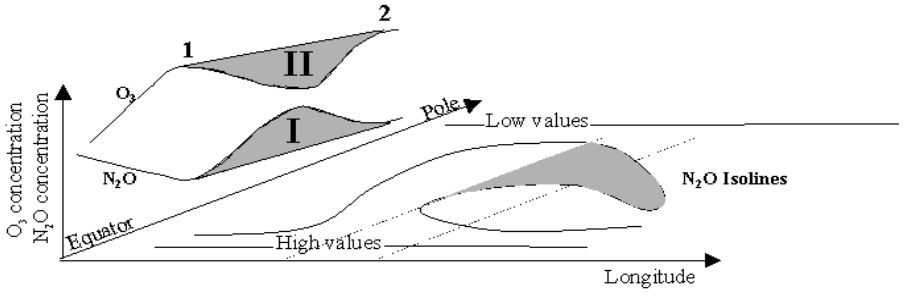

Fig. WP 5-31: Sketch of the streamer detection algorithm.

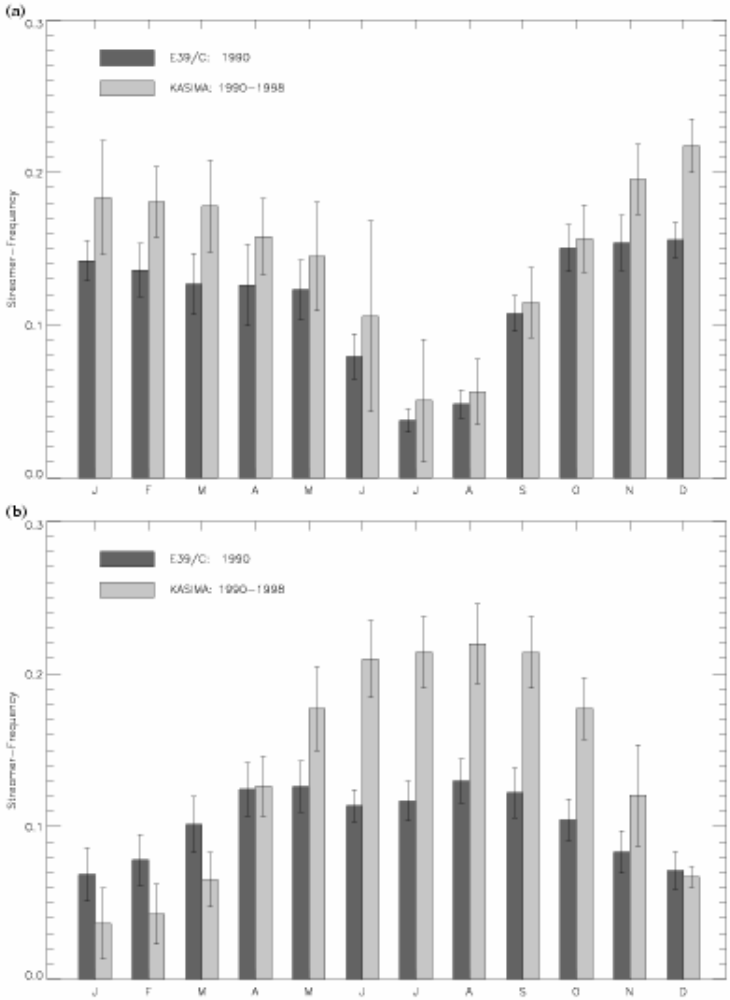

Figure WP 5-32: Seasonal cycle of streamer frequencies for KASIMA (light grey boxes) and E39/C (dark grey boxes) and the corresponding inter-annual standard deviation averaged between 21 and 25 km. The distribution is a mean streamer frequencies between 20° and 70° latitude in the northern hemisphere (a) and southern hemisphere (b).

A tropopause climatology

An important intermediate step to assessing air mass transport through the tropopause on a climatological time scale is to generate a tropopause climatology. In addition to the one to be computed with data from the CTM KASIMA, the same climatology algorithm is planned to be applied on the E39/C transient integration data (see also WP 1, joint contribution of DWD and DLR) for model validation purposes. In a preparative step, E39/C data of the "1990" scenario have been formatted to the netcdf format to be readable in the IMK routines. On this basis, climatologies of potential temperature and potential vorticity (PV) at 20, 25, and 30 km altitude have been computed using December-January-February (DJF) data from a KASIMA integration of the period 1978-1998 (nudged ECMWF analyses) and the timeslice "1990" E39/C. As an example of this first comparison the potential temperature climatologies at 25 km for the KASIMA (left) and the E39/C data are shown in figure WP 5-33.

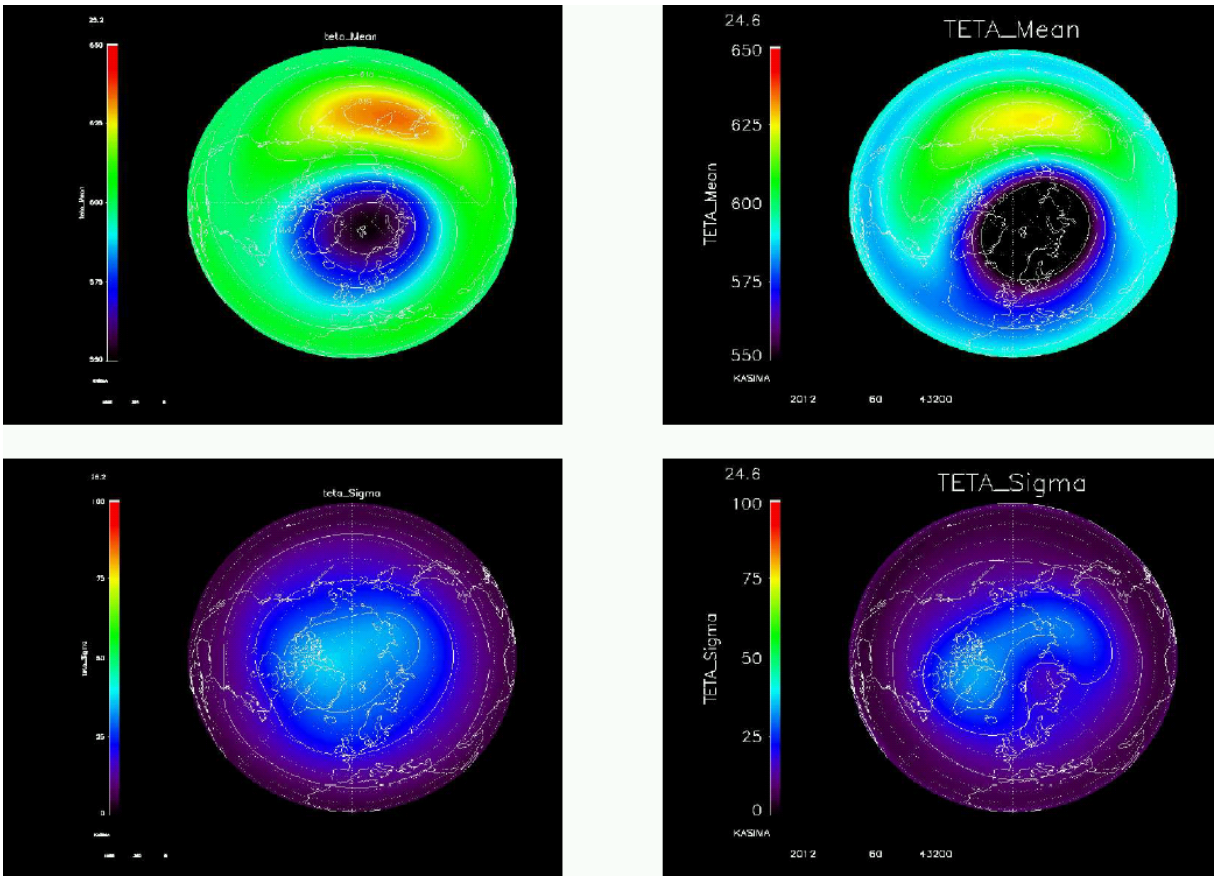

Fig. WP 5-33: DJF climatologies of potential temperature (K) at 25 km altitude. Left: KASIMA 1978-1998 integration (nudged ECMWF analyses), right: E39/C "1990" scenario. The top line shows mean values, bottom line standard deviations.

The comparison shows that E39/C reproduces the mid-stratospheric pattern of potential temperature of the wintertime northern hemisphere (top part): the region of low potential temperature values above the pole indicates the polar vortex, high values are found in the region of the Aleutian High. However, E39/C obviously generally simulates lower potential temperature values than KASIMA giving the impression for instance that the strength of the polar vortex is overestimated. Also the stratospheric variability (bottom line) is represented by the E39/C model. Over the polar region it reaches values of about half of the spatial variation of the mean values.

Because of the success in the representation of the overall middles atmosphere circulation, a 1st analysis is done with respect to the tropopause itself. Figure WP5-34 shows the mean height (top) and the standard deviation (bottom) of the height of the tropopause for the northern hemisphere winter. The tropopause is here defined by the lower surface of either the Ertels Potential Vorticity (2 PVU) in extra-tropics and the potential temperature (380 K) in the tropics. The E39/C model represents the high tropopause in the tropics, a steep wavy gradient in the region of the subtropical jet stream, and an almost flat tropopause in high latitudes. The variability is of the order of 1500 m where the tropopause is given by the EPV and considerably smaller in the tropics.

The surprisingly high variability of the tropopause height over Sibiria and Canada as well as more detailed analyses will be studied in more detail in the future.

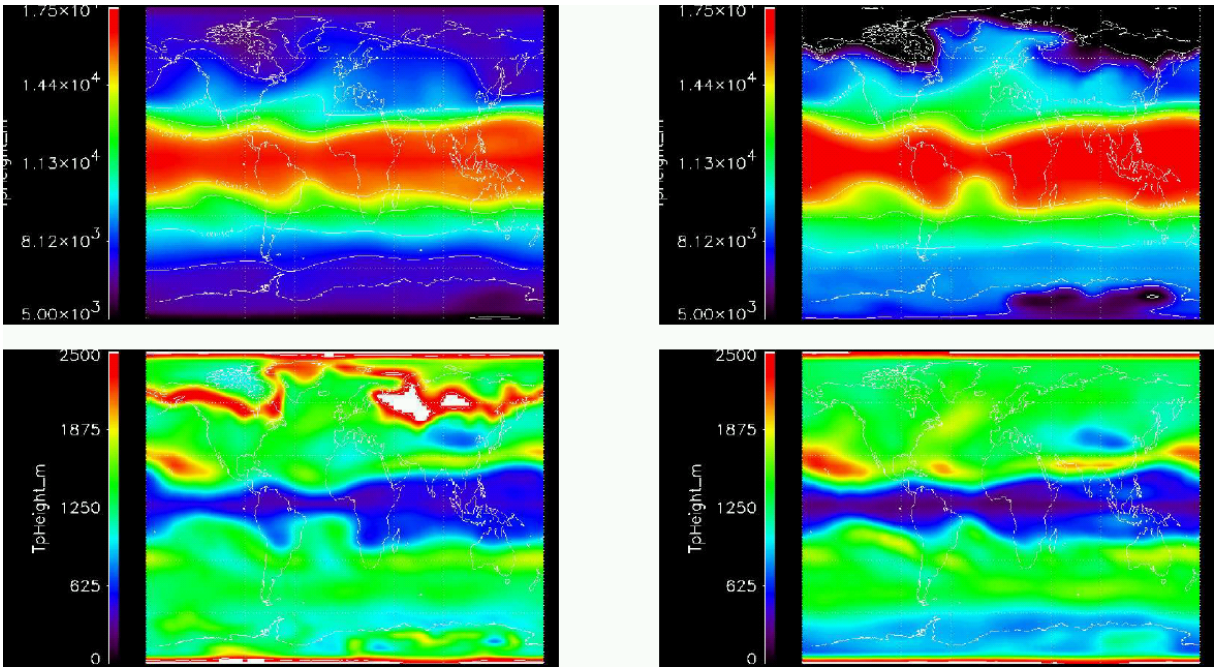

Fig. WP 5-34: As figure WP 5-33 but for the height of the tropopause.

New publications with contributions from WP5

Jöckel, P., et al., Evaluation of stratosphere-troposphere exchange and the hydroxyl radical distribution in three-dimensional global atmospheric models using observations of cosmogenic ^{14}CO, J. Geophys. Res., 107(D20), 4446, doi:10.1029/2001JD001324, 2002.

Konopka, P., H. Steinhorst, J.-U. Grooß, G. Günther, R. Müller, J. W. Elkins, H.-J. Joost, E. Richard, U. Schmidt, G. Toon and D. S. McKenna, Mixing and ozone loss in the 1999-2000 Arctic Vortex: Simulations with the three-dimensional Chemical Lagrangian Model of the Stratosphere (ClaMS), J. Geophys. Res., 2004.

Milz, M., Untersuchungen zur Messung von Wasserdampf in der tropischen Tropopausenregion mit MIPAS/Envisat, Forschungszentrum Karlsruhe, Wissenschaftliche Berichte, Bericht Nr. FZKA 6772, 2003.

Milz, M., M. Höpfner, T. von Clarmann, U. Grabowski, T. Steck, G.P. Stiller, and H. Fischer, Feasibility of measurements of water vapor and ice clouds in the tropical UT/LS region with MIPAS/ENVISAT, Adv. Space Res., 34, 815 – 819, 2004.

Steil, B., C. Brühl, E. Manzini, P.J. Crutzen, J. Lelieveld, P.J Rasch, E. Roeckner, K. Krüger, A new interactive chemistry climate model. I: Present day climatology and interannual variability of the middle atmosphere using the model and 9 years of HALOE/UARS data. J. Geophys. Res., 108(D9), 4290, doi:10.1029/2002JD002971, 2003.

PhD Thesis:

Milz, M.,Untersuchungen zur Messung von Wasserdampf in der tropischen Tropopausenregion mit MIPAS/Envisat, Universität Karlsruhe, Institut für Meteorologie und Klimaforschung, 2003.

References

Andrews, D., G., J. R. Holton, and C. B. Leovy, Middle atmosphere dynamics, academic press, international geophysics series, 1987.

Andrews, D. and M. E. McIntyre, Planetary waves in horizontal and vertical shear: The generelized Eliassen-Palm relation and the mean zonal acceleration. J. Atmos. Sci., 33, 2031-2048.

Dunkerton, T., On the mean meridional mass motions of the stratospherre and mesosphere, J. Atmos. Sci, 35, 2325-2333, 1978.

DWD, Europäischer Wetterbericht des Deutschen Wetterdienstes, 1996.

Grewe, V. and M. Dameris, Calculating the global mass exchange between stratosphere and troposphere, Ann. Geophysicae, 14, 431-442, 1996.

Holton, J. R., Haynes, P. H., McIntyre, M. E., Douglas, A. R., Rood, R. B., and Pfister, L., Stratosphere-troposphere exchange, Rev. Geophys., 121, 403-439, 1995.

James, P., A. Stohl, C. Forster, S. Eckhardt, P. Seibert, and A. Frank, A 15-year climatology of stratosphere-troposphere exchange with a Lagranggian particle dispersion model: 1. Mthology and validation, J. Geophys. Res., 108, 8519, doi:10.1029/2002JD002637, 2003.

Kouker, W., D. Offermann, V Küll, R. Ruhnke, Th. Reddmann, A. Franzen, Streamers observed by the CRISTA experiment and the KASIMA model, J. Geophys. Res, Vol. 104, pp. 16405-16418, 1999.

McKenna, D. S., P. Konopka, J.-U. Grooß, G. Günther, R. Müller, R. Spang, D. Offermann, and Y. Orsolini, A new Chemical Lagrangian Model of the Stratosphere (CLaMS): Part I Formulation of Advection and Mixing, J. Geophys. Res., 2001.

McKenna, D. S., J.-U. Grooß, G. Günther, P. Konopka, R. Müller, and G. Carver, A new Chemical Lagrangian Model of the Stratosphere (CLaMS): Part II Formulation of Chemistry Scheme and Initialisation, J. Geophys. Res., 2001.

Meloen, „J., P. Siegmund, P. Van Velthoven, H. Kelder, M. Sprenger, H. Wernli, A. Kentarchos, G. Roelofs, J. Feichter, C. Land, C. Forster, P. James, A. Stohl, W. Collins, and P. Cristofanelli, Stratosphere-troposphere exchange: A model and method intercomparison, J. Geophys. Res, 108, 8526, doi: 10.1029/2002JD002274, 2003.

Palmén, E. And C. W. Newton, Atmospheric circulation patterns, academic press, international geophysics series, 13, 603 pp, 1969.
Ray, E., Moore, F. L., Elkins, J.W., Hurst, D. F., Romashkin, P. A., Dutton, G. S. and D. Fahey, Descent and Mixing in the 1999-2000 Northern Polar Vortex inferred from in-situ Tracer Measurements, J. Geophys. Res., 2002.
Sigmond, M., J. Meloen, and P. C. Siegmund, stratospher-troposphere exchange in an extratropical cyclone, calculated with a Lagrangian method, Ann. Geophys, 18, 573-582, 2000.
Wei, M. Y., A new formulation of the exchange of mass and trace constituents between the stratosphere and the troposphere, J. Atmos. Sci, 44, 3079-3086, 1987.
Wirth, V. And J. Eggger, Diagnosing extratropical synoptic-scale stratosphere-troposphere exchange, Q. J. R. Meteorol. Soc., 125, 635-655, 1999.